





ARTICLE

Novel phospho-switch function of delta-catenin in dendrite development

Ryan Baumert^{1,2} , Hong Ji¹, Adriana Paulucci-Holthausen¹ , Aaron Wolfe³, Cari Sagum⁴, Louis Hodgson⁵ , Jyothi Arikath⁶, Xiaojiang Chen³, Mark T. Bedford^{4,8}, M. Neal Waxham^{2,7}, and Pierre D. McCre^{1,2,8} 

In neurons, dendrites form the major sites of information receipt and integration. It is thus vital that, during development, the dendritic arbor is adequately formed to enable proper neural circuit formation and function. While several known processes shape the arbor, little is known of those that govern dendrite branching versus extension. Here, we report a new mechanism instructing dendrites to branch versus extend. In it, glutamate signaling activates mGluR5 receptors to promote Ckd5-mediated phosphorylation of the C-terminal PDZ-binding motif of delta-catenin. The phosphorylation state of this motif determines delta-catenin's ability to bind either Pdlim5 or Magi1. Whereas the delta:Pdlim5 complex enhances dendrite branching at the expense of elongation, the delta:Magi1 complex instead promotes lengthening. Our data suggest that these complexes affect dendrite development by differentially regulating the small-GTPase RhoA and actin-associated protein Cortactin. We thus reveal a “phospho-switch” within delta-catenin, subject to a glutamate-mediated signaling pathway, that assists in balancing the branching versus extension of dendrites during neural development.

Introduction

The immensely complex network of synaptic connections in the brain is highly dependent on the proper development, function, and maintenance of dendrites. Dendrites are largely responsible for receiving signals from other neurons and undergo numerous branching and elongation events throughout their development. Abnormal dendrite morphology contributes to atypical synaptic connectivity and has been associated with the cognitive deficits of many neurodevelopmental disorders (Kaufmann and Moser, 2000; Cerruti Mainardi, 2006; Martínez-Cerdeño, 2017).

Dendrite development is largely governed by the modulation of intracellular pathways by extracellular signaling cues (Dong et al., 2015). Namely, the neurotransmitter glutamate has been strongly implicated in the establishment of dendritic morphology (Portera-Cailliau et al., 2003; Park et al., 2007; Ballester-Rosado et al., 2010). Cultured primary hippocampal neurons treated with glutamate develop significantly more complex dendritic arbors when compared with controls, whereas blocking activity of glutamate receptors results in the formation of less complex dendritic arbors (Charych et al., 2006; Hamad et al., 2011; Previtara and Firestein, 2015). Both hippocampal

and cortical neurons of mice lacking *Grm5*, the gene that encodes the glutamate receptor mGluR5, develop significantly less complex dendritic arbors than controls in vivo (Ballester-Rosado et al., 2010; Loerwald et al., 2015). Further, cultured neurons treated with the type 1 mGluR (mGluR1 and mGluR5) agonist 3,5-dihydroxyphenylglycine (DHPG) exhibit increased dendrite growth during early development (Cruz-Martín et al., 2012). Despite the extensive evidence for glutamate and its metabotropic receptor's roles in dendrite development, surprisingly little is known about the mechanisms downstream of its signaling in dendrites. We investigate mechanistic changes elicited by glutamate signaling, specifically through the receptor mGluR5. Our findings implicate the neural catenin protein delta-catenin in controlling dendritic development following mGluR5 activation.

Delta-catenin is a member of the p120-catenin family of catenin proteins, which bind the cytoplasmic region of cadherin proteins as part of the cadherin-catenin adhesion complex (Zhou et al., 1997; Yuan et al., 2015). In addition to the armadillo domain present in all p120-catenin family members, delta-catenin

¹Department of Genetics, The University of Texas MD Anderson Cancer Center, Houston, TX; ²Program in Neuroscience, The University of Texas Graduate School of Biomedical Science, Houston, TX; ³Computational Biology and Norris Comprehensive Cancer Center, University of Southern California, Los Angeles, CA; ⁴Department of Epigenetics and Molecular Carcinogenesis, The University of Texas MD Anderson Cancer Center, Smithville, TX; ⁵Department of Anatomy and Structural Biology and Gruss-Lipper Biophotonics Center, Albert Einstein College of Medicine, Bronx, NY; ⁶Department of Anatomy, Howard University, Washington, DC; ⁷Department of Neurobiology and Anatomy, The University of Texas Health Science Center at Houston McGovern Medical School, Houston, TX; ⁸Program in Genetics and Epigenetics, The University of Texas Graduate School of Biomedical Science, Houston, TX.

Correspondence to Pierre D. McCre: pdmccrea@mdanderson.org; Ryan Baumert: rbaumert@mdanderson.org.

© 2020 Baumert et al. This article is distributed under the terms of an Attribution–Noncommercial–Share Alike–No Mirror Sites license for the first six months after the publication date (see <http://www.rupress.org/terms/>). After six months it is available under a Creative Commons License (Attribution–Noncommercial–Share Alike 4.0 International license, as described at <https://creativecommons.org/licenses/by-nc-sa/4.0/>).

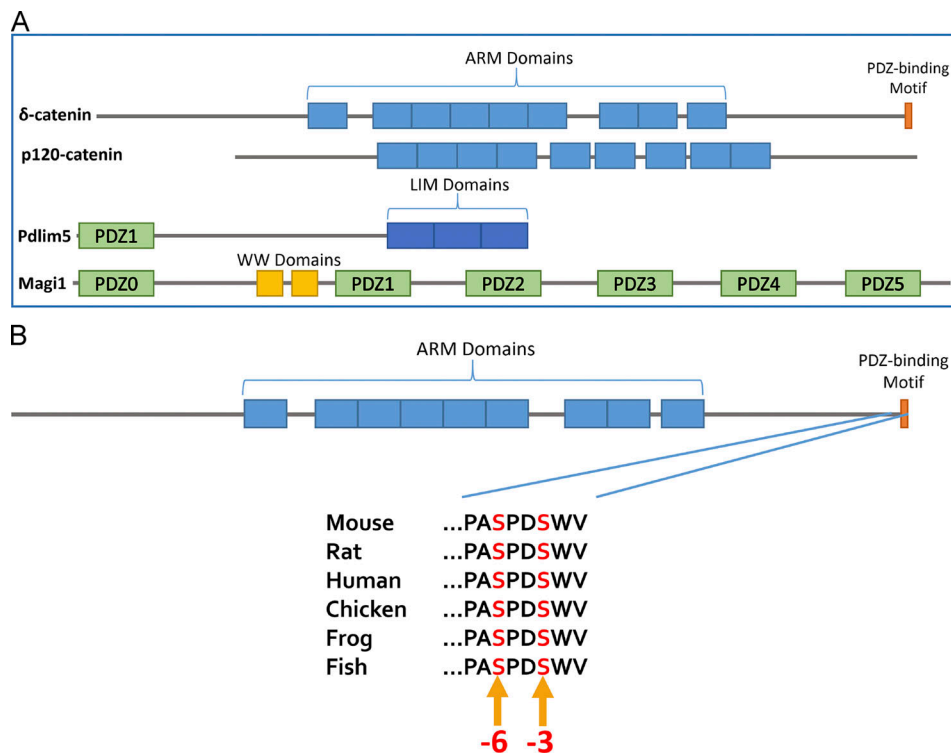


Figure 1. **Illustration of domains within delta-catenin, Magi1, and Pdlim5.** (A) Schematics of the proteins delta-catenin, p120-catenin, Pdlim5, and Magi1. (B) Conservation of the C-terminus of delta-catenin across species.

also contains a highly conserved PDZ-binding motif, which recognizes and binds numerous PDZ domain-containing proteins crucial for neural development (Fig. 1, A and B; Yuan et al., 2015). Proteomic analysis of the developing rat brain has revealed a pair of phosphorylation sites (S1245 and S1242) within the PDZ-binding motif of delta-catenin (Lundby et al., 2012). As elucidated here, we propose that phosphorylation of these sites on delta-catenin plays an important role in determining delta-catenin's role in neuronal development.

Perturbations in the normal functioning of delta-catenin have been linked to several neurodevelopmental disorders, such as cri-du-chat syndrome, autism, and schizophrenia (Medina et al., 2000; Vrijenhoek et al., 2008; Turner et al., 2015). In neurons, delta-catenin is required for proper dendrite development, as shRNA-mediated knockdown (KD) of delta-catenin leads to inhibition of both dendrite elongation and branching, while overexpression of delta-catenin results in increased dendritic length and complexity (Martinez et al., 2003; Arikath et al., 2008). Overexpression of delta-catenin in NIH/3T3 cells, among other nonneuronal cell lines, induces the formation and branching of dendrite-like processes through the remodeling of actin and microtubules (Kim et al., 2002; Kim et al., 2008a). There is evidence that these roles of delta-catenin in dendrite growth are dependent upon its PDZ-binding motif, as loss of this region prevents the increased dendritic arborization induced by delta-catenin overexpression in neurons (Arikath et al., 2008). Here, we reveal a pair of novel interactions between the PDZ-binding motif of delta-catenin and the proteins Magi1 and Pdlim5 and provide

mechanistic insight into the processes underlying dendrite development.

Magi1 is a neural member of the membrane-associated guanylate kinase, or MAGUK, subfamily of PDZ proteins and contains six PDZ domains, a GUK domain, and two WW motifs (Fig. 1 A). The PDZ domains of MAGUK proteins are linked to the adhesive and scaffolding roles of these proteins and are crucial for many aspects of neuronal development and function, including dendritogenesis and synaptogenesis (Montgomery et al., 2004; Oliva et al., 2012). In neurons, Magi1 localizes to the growth cones of developing neurites, while in PC12 rat pheochromocytoma cells, RNAi-mediated KD of Magi1 leads to a loss of nerve growth factor-induced neurite outgrowth (Ito et al., 2013). Magi1 copy number variation has also been associated with both bipolar disorder and schizophrenia, providing further evidence of the protein's significance in neuronal development (Karlsson et al., 2012; de Moor et al., 2015). Despite these findings on the involvement of Magi1 in neurite extension, the mechanisms underlying the protein's role in dendritogenesis remain unclear.

Pdlim5 is a PDZ protein that has enriched expression in neural tissues and contains one PDZ domain and three LIM (Lin11, Isl-1, and Mec-3) domains (Fig. 1 A) and, like Magi1, localizes to the growth cones of neurite tips in primary neuron cultures. However, while Magi1 is thought to contribute to neurite outgrowth, Pdlim5 has been found to promote growth cone collapse via the translocation of PKCε to the membrane, as well as to restrict dendritic spine growth through an interaction with spine-associated Rap GTPase-activating protein (SPAR;

Herrick et al., 2010; Ren et al., 2015). Pdlim5 has also been implicated in the progression of several neurological conditions, including schizophrenia, bipolar disorder, and major depression, although its role in the onset of these maladies remains unclear (Kato et al., 2005; Horiuchi et al., 2006, 2013).

As described here, despite the seemingly opposing roles of Magi1 and Pdlim5 in neurite/dendrite development, each interacts with the PDZ-binding motif of delta-catenin. Importantly, we find that formation of one complex versus the other is determined by the phosphorylation status of delta-catenin's PDZ-binding motif. In response to the neurotransmitter glutamate and Cdk5 kinase, we provide evidence that the formation of these complexes dynamically modulates dendritic elongation (delta:Magi1 complex) versus branching (delta:Pdlim5 complex). We refer to this mechanism, centered within delta-catenin's PDZ-binding motif, as a phospho-switch. Given the established roles of glutamate, Cdk5, and delta-catenin in dendrite elaboration, in combination with our findings described below, delta-catenin's phospho-switch is likely to be instrumental in dendrite development, and potentially in disease.

Results

Delta-catenin contributes to the *in vitro* morphogenesis of hippocampal neurons

Given the reported roles of delta-catenin in neuronal development and dendrite morphology, we aimed to address mechanisms by which this protein functions in neurons. Primary rat hippocampal neurons were transfected at 3 d *in vitro* (DIV) and fixed at 7 DIV. Primary neuronal cultures provide an ideal model system, as they can be subjected to a greater variety of manipulations than their *in vivo* counterparts, while still largely mirroring the development of neurons *in vivo*. The rationale for choosing 7 DIV as a stop point is that at 7 DIV the dendritic tree is already quite complex, yet very few synapses have started to form. This enables us to address dendrite morphology before synaptic changes becoming an additional driving force behind observed alterations. In developing neurons subject to delta-catenin KD (shRNA-mediated initiated at 3 DIV), the dendritic tree was restricted when compared with both control and delta-catenin overexpressing neurons at 7 DIV (Fig. 2, A–C). While dendrite lengths were significantly reduced, the overall number of dendrites was left relatively unchanged. When delta-catenin was instead exogenously expressed (initiated at 3 DIV), dendritic trees showed heightened complexity as well as length compared with controls (7 DIV; Fig. 2, A–C). Sholl analysis confirmed that the increase in dendrite density is maintained across the length of the dendritic arbor (Fig. 2 D). Together, our results support prior studies that dendrite branching and elongation are modulated by delta-catenin (Martinez et al., 2003; Arikath et al., 2008).

Phosphorylation of the PDZ-binding motif of delta-catenin modulates dendritic morphology

The PDZ-binding motif of delta-catenin contains two conserved phospho-serines at its extreme C-terminus (e.g., mouse S1242 and S1245; Fig. 1 B) that importantly can be phosphorylated

in vivo (Lundby et al., 2012). To facilitate our discussion of these two serine residues across species, we refer to them as residing at the –6 and –3 positions (with the –1 position being delta-catenin's C-terminal valine). Given the roles of delta-catenin in dendrite development, and published evidence that the phosphorylation of PDZ-binding motifs is able to alter some associations and functions, we investigated the role of phosphorylation at delta-catenin's –3 and –6 serines (Espejo et al., 2002; Sundell et al., 2018). This was accomplished by expressing a pair of phospho mutants of delta-catenin in hippocampal neurons. The –6 and –3 position serine residues in delta-catenin were mutated to alanine (phospho-null) or glutamate (phospho-mimic). Hippocampal neurons (7 DIV) expressing phospho-null delta-catenin developed significantly longer dendrites, with little to no change in the number of dendrites per neuron when compared with controls (Fig. 3, A–C). Conversely, when a phospho-mimic delta-catenin was expressed, neurons developed strikingly dense dendritic trees relative to controls, with little effect upon dendrite length (Fig. 3, A–C). Sholl analysis revealed phospho-mimic delta-catenin-expressing neurons to have highly complex, though restricted in length, dendritic arbors when compared with phospho-null delta-catenin neurons, which exhibited less dense arbors that extended significantly farther out from the soma (Fig. 3 D). We observed no differences in localization within dendrites between the two delta-catenin mutants (Fig. S1), suggesting that these phosphorylation events do not serve to re-localize delta-catenin, but rather that they modify its functions in specific cellular regions.

Glutamate signaling initiates phosphorylation of delta-catenin's PDZ-binding motif and influences dendrite development

Because the phospho-mimic (SS>EE) and phospho-null (SS>AA) mutants of delta-catenin's PDZ-binding motif exhibited notably distinct effects upon dendrite development (Fig. 3), we evaluated the phosphorylation state of endogenous delta-catenin within its PDZ-binding motif and then sought to identify factors relevant to such phosphorylation events in the context of dendrite development. Through visual inspection and use of the GPS 3.0 software, we had earlier identified a phospho-MAPK/CDK consensus site centered at the –6 serine position within the PDZ-binding motif of delta-catenin (Fig. 1 B). To detect endogenous phosphorylation of delta-catenin's PDZ-binding motif, we made sequential use of two proven commercially available antibodies (see Materials and methods). This allowed us to detect and quantify phosphorylation of delta-catenin's PDZ-binding motif at the –6 serine position (Fig. 4 A). We find that ~3% of total neuronal delta-catenin is phosphorylated at this site, indicating that this event occurs selectively in neurons (Fig. 4 B). Exposure of hippocampal neuron cultures to the type 1 mGluR agonist, DHPG, stimulated phosphorylation of delta-catenin's PDZ-binding motif. Following treatment of 7-DIV hippocampal neurons (20 μ M DHPG; 10 min), delta-catenin was phosphorylated at levels over eightfold higher than control neurons (Fig. 4, C and E). Conversely, treatment of hippocampal cultures with an mGluR5 antagonist, 3-((2-methyl-1,3-thiazol-4-yl)ethynyl)pyridine

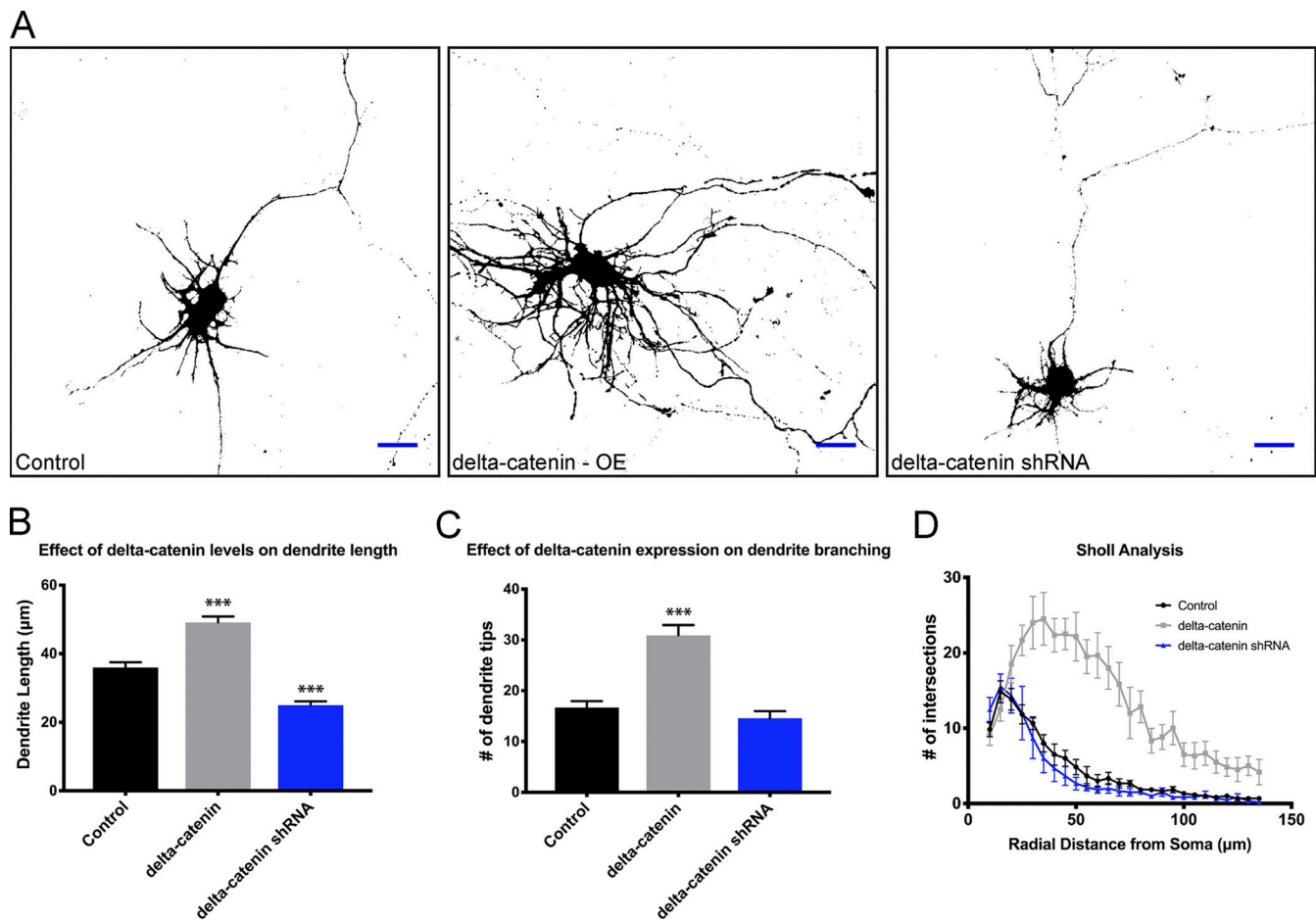


Figure 2. Delta-catenin plays a major role in the establishment of hippocampal neuron dendrite morphology. (A) Representative images of 7-DIV rat hippocampal neurons expressing GFP, delta-catenin cDNA, and delta-catenin shRNA. (B) Quantification of average dendrite length of neurons expressing GFP ($35.96 \pm 1.56 \mu\text{m}$), delta-catenin cDNA ($49.14 \pm 1.72 \mu\text{m}$; $P < 0.0001$), and delta-catenin shRNA ($24.98 \pm 1.13 \mu\text{m}$; $P < 0.0001$). (C) Average dendrite density of neurons expressing GFP (16.69 ± 1.26), delta-catenin cDNA (30.90 ± 2.03 ; $P < 0.0001$), and delta-catenin shRNA (14.56 ± 1.43 ; $P < 0.0001$). (D) Sholl analysis of dendrite morphology for control, delta-catenin overexpressing, and delta-catenin shRNA-expressing neurons. Relative to GFP-expressing cells, neurons overexpressing delta-catenin possessed significantly more dendrites at 25–70 μm from the soma ($P \leq 0.0001$) and from 70 to 110 μm from the soma ($P < 0.05$). $***$, $P \leq 0.0001$. Error bars indicate SEM. For B and C, $n \geq 12$ neurons; for D, $n = 6$. For B and C, significance was determined using a one-way ANOVA followed by Tukey’s test. For D, a two-way ANOVA with Bonferroni post-hoc analysis was used. Scale bars, 20 μm .

(MTEP), produced a 42% decrease in the relative levels of phosphorylated delta-catenin (Fig. 4, D and F). These observations are consistent with a pathway where metabotropic glutamate receptors function upstream of phosphorylation of delta-catenin’s PDZ-binding motif.

We next investigated whether DHPG-induced mGluR signaling modulates dendrite morphogenesis. Primary hippocampal neurons visualized via transfection with GFP (3 DIV) as previously described were treated with DHPG at 7 DIV (20 μM ; 180 min). In agreement with published studies (Cruz-Martín et al., 2012; Previtara and Firestein, 2015), DHPG-treatment increased dendrite numbers relative to controls (Fig. 4, G–I), phenocopying our previous observations from expressing a phospho-mimic delta-catenin mutant (Fig. 3). DHPG treatment of neurons subjected to shRNA-mediated KD of delta-catenin produced no significant effect on dendrite morphology (Fig. 4, J–L). Given these agonist-induced phosphorylation and morphological responses, type 1 mGluRs appear to be well poised to

modulate phosphorylation of delta-catenin’s PDZ-binding motif and its subsequent impact on dendrite morphology.

Delta-catenin interacts with Magi1 and Pdlim5 in a phospho-dependent manner

Given the observed switch-like function of delta-catenin in dendrite development, we sought to identify neuronal interaction partners of delta-catenin that might help explain the contrasting roles of delta-catenin in the elaboration of dendrite morphology. Based upon the literature, a number of neuronal functions of delta-catenin have been linked to the association of its PDZ-binding motif with proteins bearing PDZ domains (Ide et al., 1999; Arikath et al., 2008; Yuan et al., 2015). Interestingly, in unrelated studies, the phosphorylation of PDZ-binding motifs has in some cases been found to alter their interactions (Chung et al., 2000; Lee and Zheng, 2010; Espejo et al., 2017). We chose to use protein-domain microarrays to reveal novel PDZ-domain proteins that bind to delta’s PDZ-binding motif and to

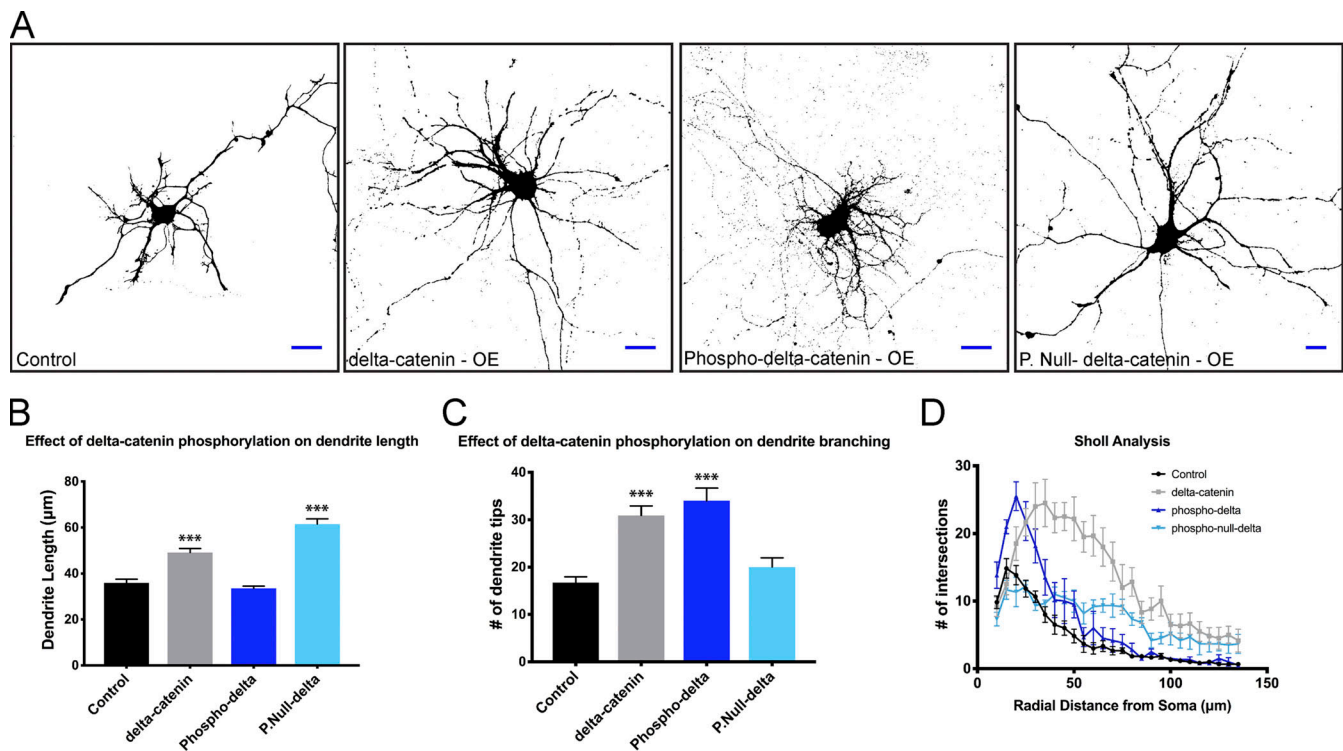


Figure 3. Point mutants that mimic phosphorylation (versus lack thereof) within the PDZ-binding motif of delta-catenin suggest a role of this modification in directing dendritic morphology. (A) Representative images of 7-DIV rat hippocampal neurons transfected with GFP (control), delta-catenin cDNA, delta-catenin-EE (phospho-mimic) cDNA, and delta-catenin-AA (phospho-null/P.Null) cDNA. OE, overexpression. (B) Quantification of average dendrite length of neurons expressing GFP ($35.96 \pm 1.56 \mu\text{m}$), delta-catenin cDNA ($49.14 \pm 1.72 \mu\text{m}$; $P < 0.0001$), delta-catenin-EE (phospho-mimic) cDNA ($33.59 \pm 0.90 \mu\text{m}$; $P = 0.601$), and delta-catenin-AA (phospho-null) cDNA ($61.50 \pm 2.286 \mu\text{m}$; $P < 0.0001$). (C) Average dendrite density of neurons expressing GFP (16.69 ± 1.26), delta-catenin cDNA (30.90 ± 2.03 ; $P < 0.0001$), delta-catenin-EE (phospho-mimic) cDNA (34.00 ± 2.65 ; $P < 0.0001$), and delta-catenin-AA (phospho-null) cDNA (20.00 ± 1.96 ; $P = 0.601$). (D) Sholl analysis of dendrite morphology for control, delta-catenin-overexpressing, phospho-mimic delta-catenin-overexpressing, and phospho-null delta-catenin-overexpressing neurons. Relative to GFP-expressing cells, neurons overexpressing phospho-mimic delta-catenin possessed significantly more dendrites at 15–35 μm from the soma ($P < 0.05$). Conversely, neurons overexpressing phospho-null delta-catenin possessed significantly more dendrites at 60–80 μm ($P < 0.05$) relative to GFP controls. ***, $P \leq 0.0001$. Error bars indicate SEM. For all conditions in A–C, $n \geq 12$ neurons; in D, $n = 6$. For B and C, significance was determined using a one-way ANOVA followed by Tukey’s test. For D, a two-way ANOVA with Bonferroni post-hoc analysis was used. Scale bars, 20 μm .

test if phosphorylation at the –6 and/or –3 serine positions of delta has an impact upon such interactions. 98 individually purified PDZ domains that had demonstrated peptide binding activity (Stiffler et al., 2006), from 68 different human proteins, were arrayed by the MD Anderson Cancer Center (MDACC) Protein Array and Analysis Core facility and probed with biotinylated unphosphorylated versus phosphorylated delta-catenin peptide inclusive of its PDZ-binding motif (Fig. 5 A). The data pointed to a number of interactions, including positive controls that helped to validate our screen (e.g., Erbin and Magi2; Ide et al., 1999; Arikkath et al., 2008). Given our interest in potential phospho-regulation of delta-catenin’s PDZ-binding motif in the context of dendrite morphology, we focused upon a novel pair of phospho-regulated interactions that were revealed, namely with the final PDZ domain present in Magi1 (PDZ5), as well as with the sole PDZ domain in Pdlim5, both of which have established roles in neuron/dendrite development and/or function (Ito et al., 2012, 2013; Ren et al., 2015; Fig. 1). Using the PDZ-domain arrays, we found that the unphosphorylated PDZ-binding motif probe bound to the final PDZ5 domain of Magi1 (pair of blue-circled green spots in Fig. 5 B, left panel), and

importantly, that the phosphorylated probe instead displayed very little Magi1 association (empty blue oval in Fig. 5 B, right panel; Fig. 5, B and C). These results are consistent with our earlier experiments using yeast two-hybrid screens with delta-catenin as bait to probe a mouse brain cDNA library. Two independent clones of Magi1 containing the same PDZ5 domain were identified, generating additional interest in Magi1 (Hybrigenics Inc.; results not shown). Using the same PDZ-domain arrays as above, we noted that the opposite phospho-dependent behavior was seen for the lone PDZ domain present within Pdlim5 (red-circled regions of Fig. 5 B, left versus right panels; Fig. 5, B and C). A full table of domains probed is available in Table S1. While several other proteins displayed PDZ domains able to bind delta-catenin’s phosphorylated PDZ-binding motif in vitro (e.g., Erbin), Pdlim5 was the only target observed to require the PDZ-binding motif of delta-catenin to be phosphorylated for an interaction to occur. We found that delta-catenin’s PDZ-binding motif binds best to Pdlim5 when the –6 and –3 serines of delta are phosphorylated, although phosphorylation of even a single serine promotes binding (white-paired spots indicates higher association than green; Fig. 5 D).

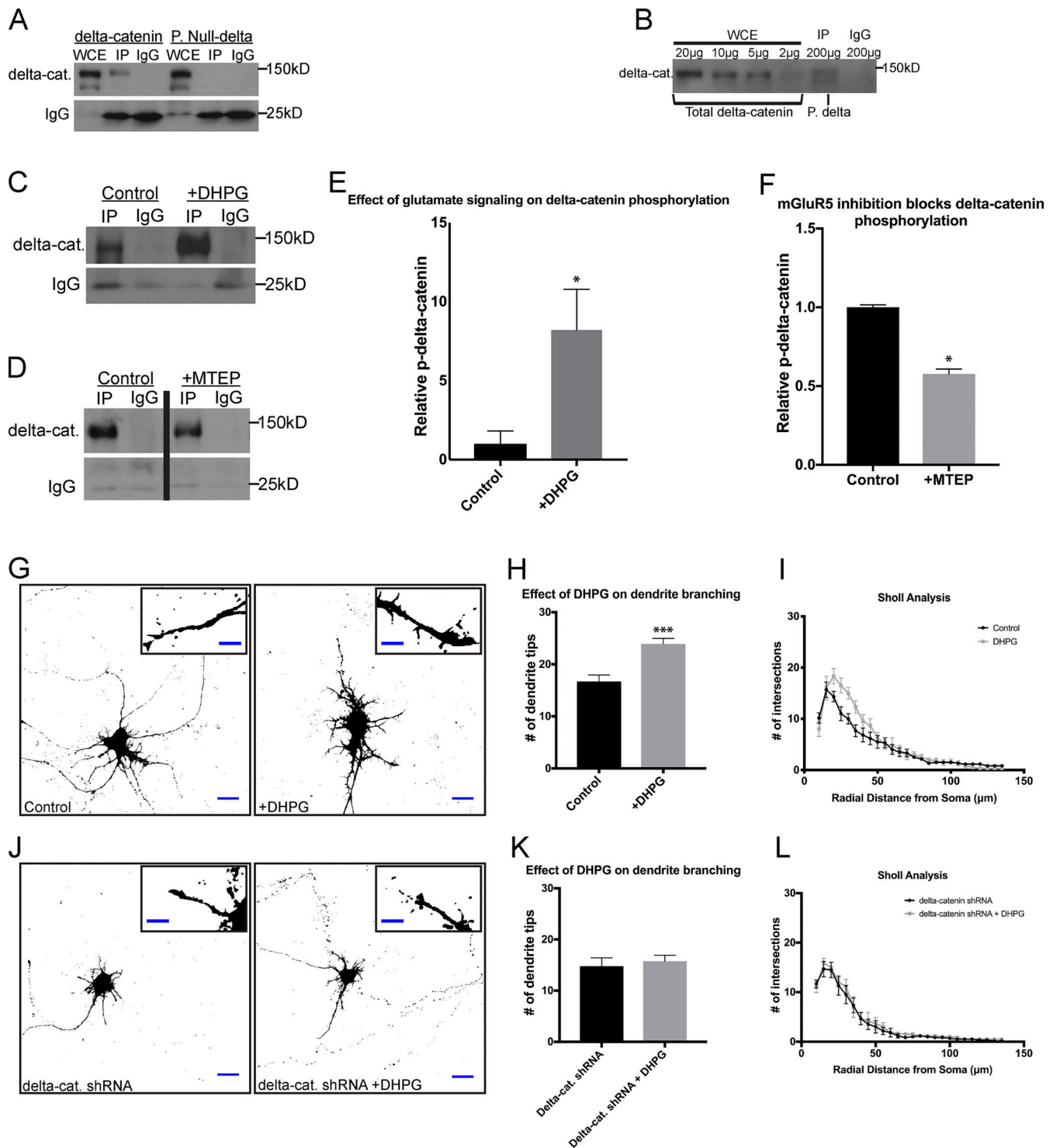


Figure 4. **Glutamate signaling is sufficient to drive phosphorylation of delta-catenin and influence its role in GTPase modulation and dendrite development.** (A) Validation of specificity of detection method for phosphorylated delta-catenin. Immunoblot images of HEK293 cells transfected with WT delta-catenin and delta-catenin-AA (phospho-null) cDNA. (B) Immunoblots of total delta-catenin and immunoprecipitated phospho-delta-catenin from 7-DIV rat hippocampal cells. We estimate that phospho-delta represents ~3% of total delta-catenin in neurons. (C) Immunoblots of immunoprecipitated phospho-delta-catenin from 7-DIV rat hippocampal cells following treatment with DHPG (20 µM; 10 min) versus no treatment. (D) Immunoblots of immunoprecipitated phospho-delta-catenin from 7-DIV rat hippocampal cells following treatment with MTEP (25 µM; 10 min) versus no treatment. (E) Quantification of fold change in delta-catenin phosphorylation following DHPG treatment in 7-DIV rat hippocampal cells. Treatment of 7-DIV cultures with 20 µM DHPG for 10 min produced an 8.202-fold increase in relative levels of phosphorylated delta-catenin compared with controls ($P = 0.0373$); graph represents cultures from four independent experiments. (F) Quantification of fold change in delta-catenin phosphorylation following MTEP treatment in 7-DIV rat hippocampal cells. Treatment of 7-DIV cultures with 25 µM MTEP for 10 min resulted in a 42% reduction in relative levels of phosphorylated delta-catenin compared with controls ($P = 0.0069$); graph represents cultures from two independent experiments. (G) Representative images of 7-DIV rat hippocampal neurons transfected with GFP and subjected to

no treatment or 20 μ M DHPG for 6 h. For each condition image, representative close-ups of dendritic branches are shown. **(H)** Quantification of dendritic density following DHPG treatment (23.92 ± 1.06 ; $P = 0.0002$). $n \geq 12$ neurons. **(I)** Sholl analysis of dendrite morphology for control and DHPG-treated neurons. Neurons treated with DHPG developed significantly more dendrites than GFP controls at 20–35 μ m from the soma ($P < 0.05$); $n = 6$. **(J)** Representative images of 7-DIV rat hippocampal neurons expressing delta-catenin shRNA and subjected to no treatment or 20 μ M DHPG for 6 h. For each condition image, representative close-ups of dendritic branches are shown. **(K)** Quantification of dendritic density in neurons expressing delta-catenin shRNA following DHPG treatment (15.75 ± 1.18 ; $P = 0.6422$). $n \geq 9$ neurons. **(L)** Sholl analysis of dendrite morphology for control and DHPG-treated neurons expressing delta-catenin shRNA. DHPG treatment did not significantly alter dendritic morphology in neurons lacking delta-catenin; $n = 6$. For E, F, H, and K, significance was determined with a two-tailed *t* test. For I and L, a two-way ANOVA with Bonferroni post-hoc analysis was used. *, $P < 0.05$; ***, $P \leq 0.0001$. Error bars indicate SEM. Scale bars, 20 μ m in G and J and 5 μ m in their respective magnified insets. IP, immunoprecipitation. WCE, whole cell extract.

The phospho-dependency of these interactions was further validated using a Golgi co-relocalization assay (GRA) we developed (see Materials and methods). For our application of this assay, delta-catenin was ectopically localized to the Golgi through its fusion (N-terminal) to a Golgi-localization tag. Then, we probed for Magi1 or Pdlim5 to reveal if either is similarly relocalized (“comes along for the ride”) to the Golgi, which would be supportive of an interaction. To probe both the phospho- and phospho-null states of the PDZ-binding motif of delta-catenin, we generated point mutants in which delta-catenin’s –6 and –3 serines were replaced either with glutamate (phospho-mimic) or alanine (phospho-null). Following the expression of phospho-null delta-catenin in HEK293 cells—which lack endogenous delta-catenin—we observed that coexpressed Magi1 nicely co-relocalized to the Golgi from the cell cytosol and membrane (Fig. 5, E and H). This same phospho-null delta-catenin construct failed to co-relocalize coexpressed Pdlim5 (Fig. 5, F and H). Conversely, when phospho-mimic delta-catenin was directed to the Golgi, it was Magi1 that failed to co-relocalize, whereas Pdlim5 succeeded in co-relocalizing to the Golgi with delta-catenin (Fig. 5, E–H). Thus, our in-cell GRA findings support the same binding selectivity shown in our in vitro protein-domain micro-arrays. They also provide some confidence, in combination with later findings, that our delta-catenin point mutants mimic the phospho- versus dephosphorylated forms of delta-catenin’s PDZ-binding motif.

Using our GRA as a readout, we further mapped the regions of Magi1 and Pdlim5 required to bind delta-catenin (Fig. S2). Our findings further supported the microarray results, since the sole PDZ domain of Pdlim5, as well as the final PDZ5 domain of Magi1, were required for the respective interaction and co-relocalization of Pdlim5 and Magi1 with delta-catenin.

Delta-catenin interacts with Magi1 and Pdlim5 during hippocampal neuron development

Pdlim5 and Magi1, like delta-catenin, are each expressed in hippocampal neurons during dendrite development. While delta-catenin is ubiquitously expressed by 7 DIV, Magi1 and Pdlim5 exhibit enriched localization to dendrites (Fig. 6 A). Specifically, at 7 DIV, Magi1 protein appears to be enriched at the tips of dendrites, with lower amounts present elsewhere in dendrites and soma. Pdlim5 is present in the soma but enriched in dendrites, with the highest visualization in dendrite tips. In mature hippocampal neurons (28 DIV), Pdlim5 protein is still present in dendrites, whereas Magi1 expression increases in the soma. Expression of all three proteins appears to steadily increase until neuronal maturity (Fig. S3). The coordinate presence of delta-catenin, Magi1, and Pdlim5 throughout much of hippocampal in vitro development, and our resolution of the

delta:Magi1 and delta:Pdlim5 protein complexes (see also below), supports the potential contribution of these interactions to dendritogenesis.

To assess whether endogenous delta-catenin interacts in primary rat hippocampal neurons with endogenous Magi1 and Pdlim5, we used proximity ligation assays (PLAs; Duolink). This method detects direct or closely apposing interactions using ligated oligonucleotide probes (Söderberg et al., 2006). At 7 DIV, hippocampal cultures exhibited significantly more PLA puncta for the delta-catenin:Magi1 and delta-catenin:Pdlim5 complexes than did negative controls (delta-catenin:c-Jun), with many of the puncta presenting on dendrites and their finer protrusions (Fig. 6, B and C).

To determine whether type 1 mGluR activation-dependent phosphorylation of delta-catenin’s PDZ-binding motif affects the presence of delta-catenin:Magi1 versus delta-catenin:Pdlim5 complexes, we used the prior-noted PLA in neuronal cultures. When 3 DIV neurons were subjected to DHPG treatment (20 μ M; 10 min), the fraction of puncta reporting on the delta-catenin:Magi1 complex decreased relative to controls (Fig. 6 D). Conversely, puncta reporting upon the delta-catenin:Pdlim5 complex were significantly increased (Fig. 6 D). This key experiment, assessing endogenous protein interactions in neurons, further implicates glutamate signaling in the phospho-dependent switch between the delta-catenin:Magi1 and delta-catenin:Pdlim5 associations during the development of neurites/dendrites.

Through the use of super-resolution stochastic optical resolution microscopy (STORM), we found that both Magi1 and Pdlim5 localize to punctated and potentially distinct filopodial-like structures present along the dendrites of hippocampal neurons (4 DIV; Fig. 6, E and F). Via STORM, delta-catenin appears localized throughout the lengths of dendrites. While both these Magi1- and Pdlim5-enriched structures occur along the length of dendrites, the Magi1 intensities appear more evident toward dendritic tips (Fig. 6 E). The observed distributions of these proteins with STORM elaborates upon the staining patterns observed with traditional confocal microscopy and may aid in revealing additional functions of Magi1/Pdlim5 in neurons. In all cases, our PLA findings in common with confocal and STORM observations support delta-catenin’s direct phosphorylation-dependent endogenous interactions with Magi1 and Pdlim5 in dendrites, consistent with functional relationships as revealed below.

Magi1 and Pdlim5 have complementary roles in regulating dendritic branching during neuronal development

We noted that neurons overexpressing Magi1 (interacts with unphosphorylated delta-catenin), much like neurons expressing

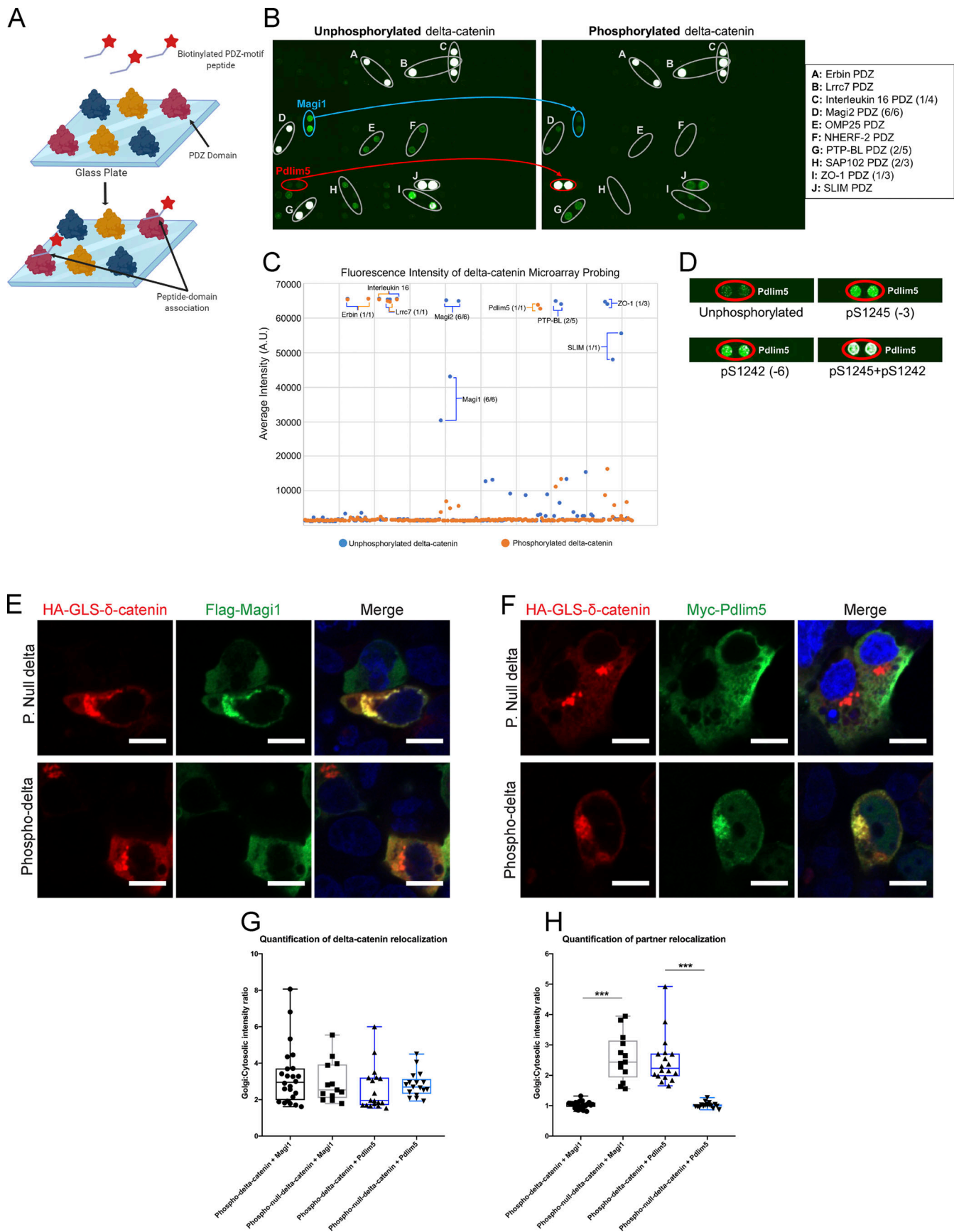


Figure 5. Delta-catenin interacts with Magi1 and Pdlim5 in a phospho-dependent manner. **(A)** Schematic of a protein-domain microarray. **(B)** Phosphorylation of the PDZ-binding motif of delta-catenin modulates the protein's ability to interact with several partner proteins. The PDZ5 domain of Magi1 is bound by the unphosphorylated motif but not by the phosphorylated motif (blue). The sole PDZ domain within Pdlim5 is bound by the phosphorylated but not unphosphorylated delta-catenin PDZ-binding motif (red). **(C)** Quantification of microarray data represented in B. **(D)** Phosphorylation at either serine in the PDZ-binding motif of delta-catenin is sufficient to allow interaction with the PDZ5 domain of Pdlim5. Phosphorylation at both sites results in a more efficacious binding of Pdlim5 by delta-catenin. **(E and F)** Test of the phospho-dependency of the Magi1:delta-catenin versus Pdlim5:delta-catenin interactions, using a GRA we developed. Mutant delta-catenin constructs (red) with phospho-null properties (S1242A, S1245A), or conversely with phospho-mimic properties (S1242E, S1245E), were expressed in HEK293 cells and relocalized to the Golgi body. **(E)** Magi1 (green) co-relocalizes to the Golgi in cells expressing phospho-null delta-catenin but not phospho-mimic delta-catenin (red). **(F)** Pdlim5 (green) co-relocalizes to the Golgi in cells expressing phospho-mimic delta-catenin but not with phospho-null delta-catenin (red). **(G)** Quantification of delta-catenin localization in GRA. **(H)** Quantification of Magi1/Pdlim5 localization in GRA. Graphs represent cultures from at least two independent experiments. ***, $P \leq 0.0001$. Box plots indicate upper and lower quartiles (top/bottom of box), median value (center line of box), and the maximum/minimum values (whiskers). For G and H, significance was determined using a one-way ANOVA followed by Tukey's test. Scale bars, 10 μm .

a phospho-null delta-catenin mutant, developed significantly longer dendrites when compared with controls, whereas dendrite density was not significantly changed (Fig. 7, A–D). Conversely, neurons overexpressing Pdlim5 (interacts with phosphorylated delta-catenin) produced dendrites with similar lengths as controls, yet with significant increases in dendritic tree density, similar to neurons expressing a phospho-mimic delta-catenin mutant (Fig. 7, E–H). In addition to overexpression studies, we used shRNA-mediated KDs beginning at 3 DIV with the fixation of neurons at 7 DIV per usual. This allowed us to determine how dendrites develop with reduced levels of Magi1 versus Pdlim5. As predicted, and nicely complementing our overexpression results, the KD of Magi1 instead significantly decreased average dendrite lengths (Fig. 7, A–D). In contrast, when neurons were knocked-down for Pdlim5, rather than a reduced density of dendrites as had been anticipated, longer dendrites formed (Fig. 7, E–H). This suggested to us that in addition to promoting branching activity in developing dendrites, Pdlim5 might participate in the inhibition of dendritic elongation. We note that these shRNA-mediated KDs were not complete (~60% for Pdlim5; Fig. S3) and thus more complete depletion might produce an effect on dendrite numbers. In any case, our current data suggest some crosstalk between the ascribed activities of Pdlim5 (branching) and Magi1 (lengthening), and/or that Pdlim5 may exercise more limited roles in early neurite formation.

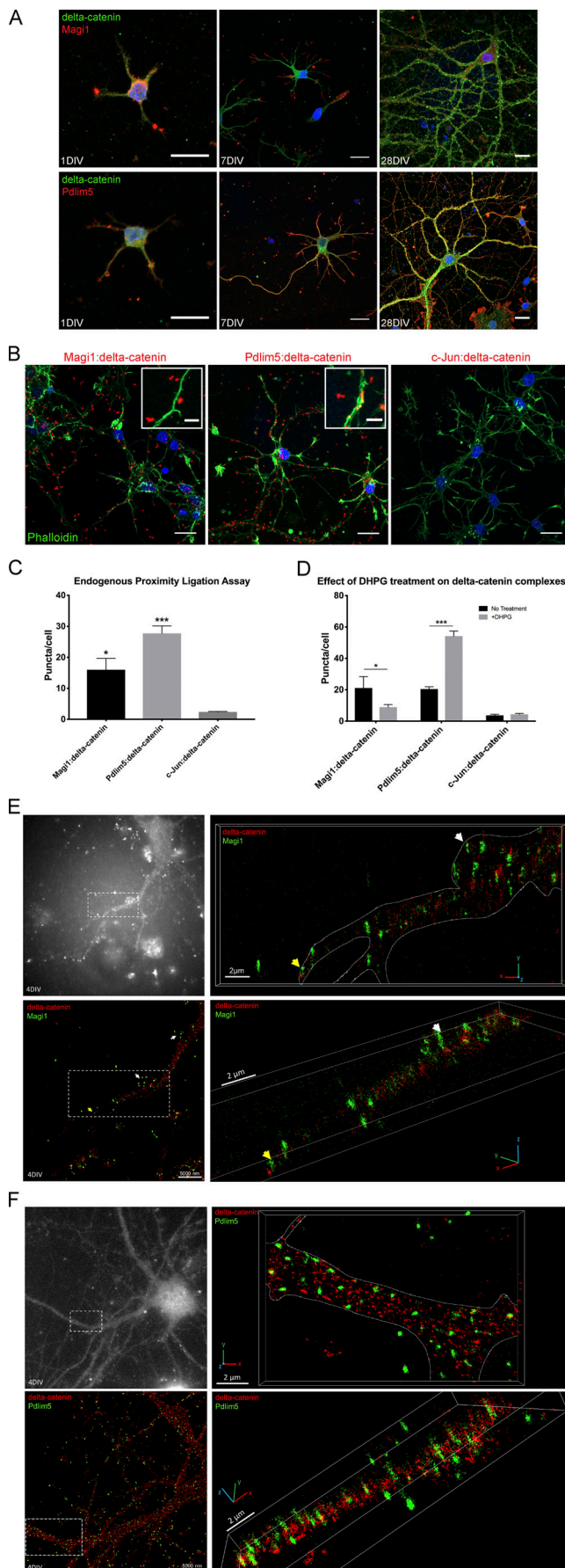
To create loss-of-function constructs of Magi1 and Pdlim5, we identified residues in the respective PDZ domains of Magi1 and Pdlim5 required to bind the dephospho versus phospho PDZ-binding motif of delta-catenin. Based on solved crystal structures of similar complexes as well as computational modeling via threading and docking simulation (see Materials and methods), we were able to view, at atomic resolution, predicted interactions of the PDZ5 domain of Magi1, or the sole PDZ domain Pdlim5, with the PDZ-binding motif of delta-catenin. Using this information, we generated double-point mutants of Magi1 (H62A, I66Y) and Pdlim5 (H63A, Q67Y), respectively, expected to be incapable of binding to the dephospho versus phospho (–6 and –3 serines) form of delta-catenin's PDZ-binding motif (Fig. 8, A–D). We named these double-point mutants Magi1-H62A/I66Y and Pdlim5-H63A/Q67Y. The loss of these mutants' ability to bind delta-catenin's PDZ ligand was confirmed in cells by using the GRA. Relative to their respective wild-type proteins,

mutant Magi1 or Pdlim5 failed to co-relocalize with delta-catenin directed to the Golgi (Fig. 8, E–H).

We then asked if the loss of Magi1's or Pdlim5's ability to bind delta-catenin altered their respective impact on dendrite development in hippocampal neurons. Indeed, exogenous Magi1-H62A/I66Y exhibited considerably less impact upon dendrite length at 7 DIV when compared with wild-type Magi1 and failed to induce dendrite elongation (Fig. 8, I–K and M). Likewise, neurons expressing exogenous Pdlim5-H63A/Q67Y showed reduced dendritic tree density relative to neurons expressing exogenous wild-type Pdlim5 (Fig. 8, I–L). While Pdlim5-H63A/Q67Y-expressing neurons did develop denser dendritic trees than GFP controls, their reduction in dendrite density relative to wild-type Pdlim5 is consistent with Pdlim5's role in dendritic branching being partially dependent on its ability to interact with delta-catenin. Consistent with these findings, both Magi1 and Pdlim5 fail to induce significant changes in dendrite morphology in neurons expressing delta-catenin shRNA (Fig. S4). Taken together, our findings from the Magi1 and Pdlim5 point mutants further support the notion that each interacts with delta-catenin as part of mechanistic pathways pertinent to the establishment of dendrite morphology in hippocampal neurons.

Delta-catenin phosphorylation is mediated by CDK5 and may modulate dendrite extension/branching through the localized inhibition of RhoA and stabilization of Cortactin

We sought to identify the kinase downstream of mGluR5, responsible for phosphorylation of delta-catenin's PDZ-binding motif. Because the PDZ-binding motif of delta-catenin contains a MAPK/CDK consensus site, we focused on select CDK or MAPK members implicated in neuron development (Cheung et al., 2007; Yamasaki et al., 2012; Liang et al., 2015). HEK293 cells were transfected with delta-catenin and CDK5 + p35 (positive-acting factor associating with CDK5), dnCDK5 + p35, or MKK7. We found that CDK5 + p35 produced the highest relative levels of PDZ-binding motif phosphorylation (15-fold increase relative to controls; Fig. 9 A). In agreement with these findings, we found that treatment of hippocampal neurons with the CDK5 inhibitor Butyrolactone I blocks DHPG-induced phosphorylation of delta-catenin in hippocampal neurons (Fig. 9 B). Taken together, our observations implicate CDK5 as a potential modulator of delta-catenin's phosphorylation-dependent association with Pdlim5 versus Magi1.



The Rho-family GTPases have well-established roles in the modulation of actin and dendrite morphology (Threadgill et al., 1997). We focused on RhoA, since it is inhibited via delta-catenin as reported in both neuronal and nonneuronal cell types (Kim et al., 2008a; Kim et al., 2008b; Zhang et al., 2014). Further, RhoA inhibition is implicated in the promotion of dendritic branching (Nakayama et al., 2000). To compare the relative levels of active RhoA across conditions, we used an ELISA-based assay (Cytoskeleton, Inc.) and extracts from HEK293 cells, since they allow facile expression of Pdlim5, Magi1, and/or delta-catenin constructs. Relative to cells expressing wild-type delta-catenin, the delta phospho-null mutant (S→A at -6 and -3 residue positions), which favors binding Magi1 (over Pdlim5), produced no change in the relative levels of active RhoA. In contrast, expression of the phospho-mimic delta-catenin (S→E at -6 and -3 positions), which favors binding to Pdlim5, significantly reduced the relative amount of active RhoA (Fig. 9 C). While the coexpression of either Magi1 or Pdlim5 with delta-catenin-amplified RhoA inhibition relative to expressing delta-catenin alone, the coexpression of Pdlim5 with delta-catenin produced the greatest inhibition of RhoA. To visualize the localization of this increased RhoA inhibition by phosphorylated delta-catenin, we used Förster resonance energy transfer (FRET)-based RhoA biosensors in primary rat hippocampal neurons (Pertz et al., 2006). Neurons expressing a phospho-mimic delta-catenin exhibited significantly

Figure 6. Delta-catenin interacts with Magi1 and Pdlim5 in developing hippocampal neurons. (A) Expression of endogenous delta-catenin (green), Magi1 (red, top), and Pdlim5 (red, bottom) in developing primary rat hippocampal neurons at 1 DIV, 7 DIV, and 28 DIV. Scale bars, 20 μ m. (B and C) Detection of direct associations between endogenous delta-catenin and the proteins Magi1 and Pdlim5 in developing hippocampal neurons. A PLA (Duolink), in combination with delta-catenin, Magi1, and Pdlim5 antibodies, was used to detect direct endogenous protein-protein interactions in 7-DIV hippocampal neurons. (B) Visualization of Magi1:delta-catenin (left) and Pdlim5:delta-catenin (center) interactions, as detected by the presence of red puncta. Insets show presence of puncta on/near small protrusions from the cell in several cases. Antibodies specific to delta-catenin and c-Jun were used in a negative control assay (right). Scale bars, 20 μ m in main panels and 5 μ m in zoomed insets. (C) Quantification of average puncta per neuron in each condition (delta-catenin+ Magi1: 16.01 [P = 0.0159]; Pdlim5: 37.73 [P = 0.0007]; c-Jun/Control: 2.393); n = 3 independent experiments. (D) Quantification of puncta/cell detected by a PLA (Duolink) in 7-DIV rat hippocampal neurons treated with DHPG. Cells were fixed immediately following treatment (no treatment versus 20 μ M DHPG; 10 min) and subjected to the assay. DHPG treatment produced an increase in Pdlim5:delta-catenin puncta relative to no treatment (54.20 \pm 3.24 vs. 20.46 \pm 1.41; P = 0.0007), while simultaneously reducing the amount of Magi1:delta-catenin complex detected per cell relative to controls (8.95 \pm 1.59 versus 21.15 \pm 7.24; P = 0.0473); n = 3 independent experiments. (E) Super-resolution confocal image of delta-catenin (red) and Magi1 (green) expression in 4-DIV primary rat hippocampal neurons. White/yellow arrows indicate Magi1 puncta near dendritic tips. Both right-hand panels are three-dimensional projection (x-y-z) views of the region outlined in the left-hand panels. (F) Super-resolution confocal image of delta-catenin (red) and Pdlim5 (green) expression in 4-DIV primary rat hippocampal neurons. Right-hand panels are x-y-z views of the region outlined in the left-hand panels. For E and F, top left panels are epi-fluorescence images of the cell/region subjected to STORM imaging. For C, significance was determined using a one-way ANOVA followed by Tukey's test. For D, a two-tailed t test was used. *, P < 0.05; ***, P \leq 0.0001. Error bars represent SEM.

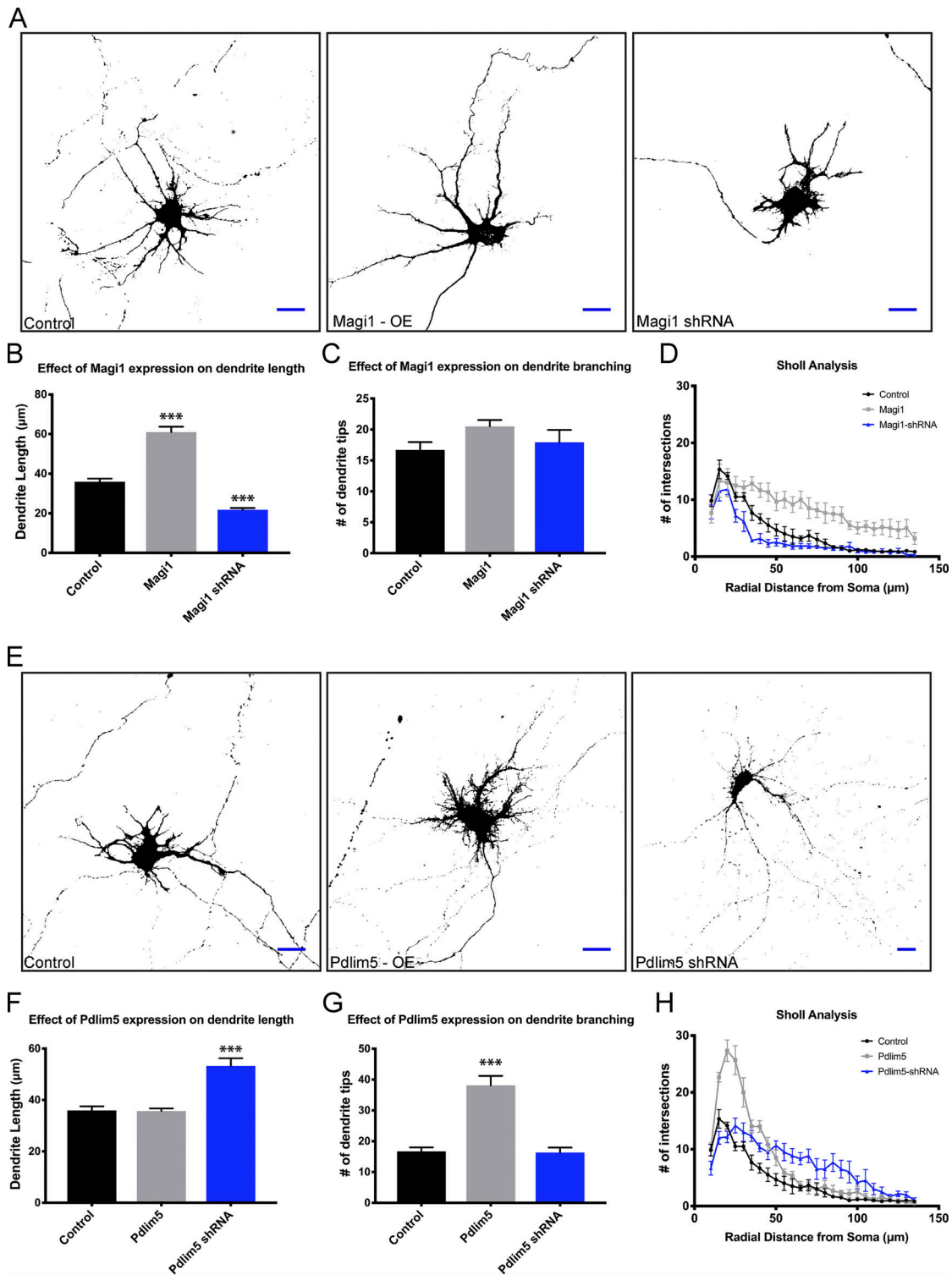


Figure 7. **Magi1 and Pdlim5 have complementary roles in dendritic branching and elongation during neuronal development.** (A) Representative images of 7-DIV rat hippocampal neurons transfected with GFP (control), Magi1 cDNA, or Magi1 shRNA. (B) Quantification of average dendrite length of neurons expressing GFP (35.96 ± 1.56 µm), Magi1 cDNA (60.98 ± 2.69 µm; P < 0.0001), and Magi1 shRNA (21.72 ± 0.98; P < 0.0001). (C) Average dendrite density of neurons expressing GFP (16.69 ± 1.26), Magi1 cDNA (20.5 ± 1.04; P = 0.132), and Magi1 shRNA (17.92 ± 2.01; P = 0.785). (D) Sholl analysis of dendrite morphology for control, Magi1-overexpressing, and Magi1 shRNA-expressing neurons. Relative to GFP-expressing cells, neurons overexpressing Magi1 possessed significantly more dendrites at 35–130 µm from the soma (P < 0.05), indicating the presence of longer dendrites. Conversely, neurons subjected to shRNA-mediated KD of Magi1 developed significantly fewer dendrites at 15 µm and 30–40 µm (P < 0.05). (E) Representative images of 7-DIV rat hippocampal neurons transfected with GFP (control), Pdlim5 cDNA, or Pdlim5 shRNA. (F) Quantification of average dendrite length of neurons expressing GFP (35.96 ± 1.56 µm), Pdlim5 cDNA (35.69 ± 1.01 µm; P = 0.9916), and Pdlim5 shRNA (53.25 ± 2.99 µm; P < 0.0001). (G) Average dendrite density of neurons expressing GFP (16.69 ± 1.26), Pdlim5 cDNA (38.13 ± 3.06; P < 0.0001), and Pdlim5 shRNA (16.33 ± 1.61; P < 0.0001). (H) Sholl analysis of dendrite morphology for control,

Pdlim5-overexpressing, and Pdlim5 shRNA-expressing neurons. Relative to GFP-expressing cells, neurons overexpressing Pdlim5 possessed significantly more dendrites at 15–40 μm from the soma ($P \leq 0.0001$). Conversely, neurons subjected to shRNA-mediated KD of Pdlim5 developed significantly more dendrites at 35–95 μm ($P < 0.05$), indicating the presence of longer dendrites. ***, $P \leq 0.0001$. Error bars indicate SEM. For all conditions in A–C and E–G, $n \geq 12$ neurons; for D and H, $n = 6$. For B, C, F, and G, significance was determined using a one-way ANOVA followed by Tukey's test. For D and H, a two-way ANOVA with Bonferroni post-hoc analysis was used. Scale bars, 20 μm . OE, overexpression.

lower RhoA activity in dendritic regions in comparison to neurons expressing a phospho-null delta-catenin mutant (Fig. 9, D–F). Our data are consistent with the possibility that the extent of downstream inhibition of RhoA, as influenced by distinct, dendritically localized delta-catenin complexes (directed by the phospho-status of delta-catenin's PDZ-binding motif), contributes to determining outcomes of dendrite branching versus elongation.

In parallel to evaluating RhoA inhibition, we identified the actin-associated protein Cortactin as an additional potential downstream effector of delta-catenin and link between delta-catenin phosphorylation and the actin cytoskeleton. Cortactin had been previously reported to associate with delta-catenin (Martinez et al., 2003; see Discussion). We found that Cortactin binds preferentially to the phospho-mimic delta-catenin mutant (as opposed to phospho-null), and that this association appears to be stabilized by overexpression of Pdlim5, as determined by coimmunoprecipitation of HEK293 cell lysates (Fig. 9, G and H). These findings suggest that when delta-catenin becomes phosphorylated and binds Pdlim5, the complex exhibits an enhanced capacity to associate with Cortactin, and potentially other actin-associated proteins, leading to the promotion of dendritic branching.

Discussion

Delta-catenin in dendrite development

Our findings promote insight upon the mechanistic changes induced by metabotropic glutamate signaling during dendrite development, positioning delta-catenin as a novel downstream component of type 1 mGluR and CDK5 kinase signal transduction. In this morphogenic pathway, delta-catenin that is unphosphorylated within its PDZ-binding motif promotes dendrite elongation, whereas delta-catenin that is phosphorylated within this motif (serines at –6 and –3 positions relative to terminal valine) instead induces dendritic branching (Fig. 10). Here, we reveal delta-catenin's novel phosphorylation-mediated binding to the PDZ-domain proteins Magil and Pdlim5, each with distinctive roles in dendrite development.

Our findings build upon previous studies that revealed that delta-catenin functions in both the elongation and branching of developing dendrites (Martinez et al., 2003; Arikath et al., 2008; Matter et al., 2009). While previous findings indicate that delta-catenin's role in dendrite development may be influenced by tyrosine and threonine phosphorylation, the significance of serine modification has remained less studied (Martinez et al., 2003; Kim et al., 2008a). It has also been reported that delta-catenin's function in dendritogenesis requires its PDZ-binding motif and association with the PDZ domain of Erbin. KD of Erbin, or deletion of the PDZ-binding motif of delta-catenin, results in the underdevelopment of dendritic trees

(Arikath et al., 2008). Our results interestingly suggest that the delta-catenin:Erbin complex is unaffected by phosphorylation of delta-catenin's PDZ-binding motif, in common with additional interactions resolved on our PDZ-domain arrays (Fig. 5, B and C). Preliminary indications are that most of delta-catenin's PDZ-motif interactions are not phospho dependent. However, as noted above, those that are may collectively contribute to wider phospho-switch effects.

Phosphorylation of delta-catenin in developing neurons

Previous analysis of phosphorylation events in the rat brain revealed that both the –6 and –3 serines of delta-catenin are phosphorylated in vivo (Lundby et al., 2012). Our findings address the regulation and function of these phosphorylation events and seek to better describe how glutamate and delta-catenin modulate dendritogenesis of hippocampal neurons, and likely that of other neuronal cells. Our data suggest that a signaling cascade initiated by type 1 metabotropic glutamate receptors (mGluR5 and mGluR1) drives phosphorylation of the –6 and –3 serines of delta-catenin. Our findings provide mechanistic insight to the role of glutamate signaling in dendrite development, which previous studies show is critical for normal dendritic branching, as blocking mGluR5 during early development results in neurons with fewer dendrites (Park et al., 2007).

Analysis of the PDZ-binding motif of delta-catenin revealed it to be a MAPK/CDK consensus sequence. Our results suggest that the kinase CDK5 may be primarily responsible for the glutamate-induced phosphorylation of delta-catenin's PDZ-binding motif. CDK5 is expressed in the growth cones of developing neurites, and loss of CDK5 function results in atypical dendrite morphology of cortical neurons (Nikolic et al., 1996; Ohshima et al., 2007). In primary hippocampal neurons, CDK5 has been shown to be required for brain-derived neurotrophic factor-induced and activity-dependent dendritic growth (Cheung et al., 2007; Liang et al., 2015). CDK5 is also activated by type 1 metabotropic glutamate receptors (mGluR5 and mGluR1) in mouse neostriatal slices (Liu et al., 2001). We propose that CDK5 functions downstream of glutamate to regulate dendritic branching via the phosphorylation of delta-catenin's PDZ-binding motif. Our findings further elaborate on the known roles of CDK5 activation in dendritic growth, though additional work is still needed to understand the extent of CDK5 activity in response to glutamate signaling, as well as to uncover additional kinases that may be responsible for the glutamate-dependent phosphorylation of delta-catenin's PDZ-binding motif during dendrite morphogenesis.

While we have yet to determine the source of glutamate in this pathway, there are several known possibilities. Neurons cocultured with glial cells develop significantly more complex dendritic arborizations than those grown under glia-free

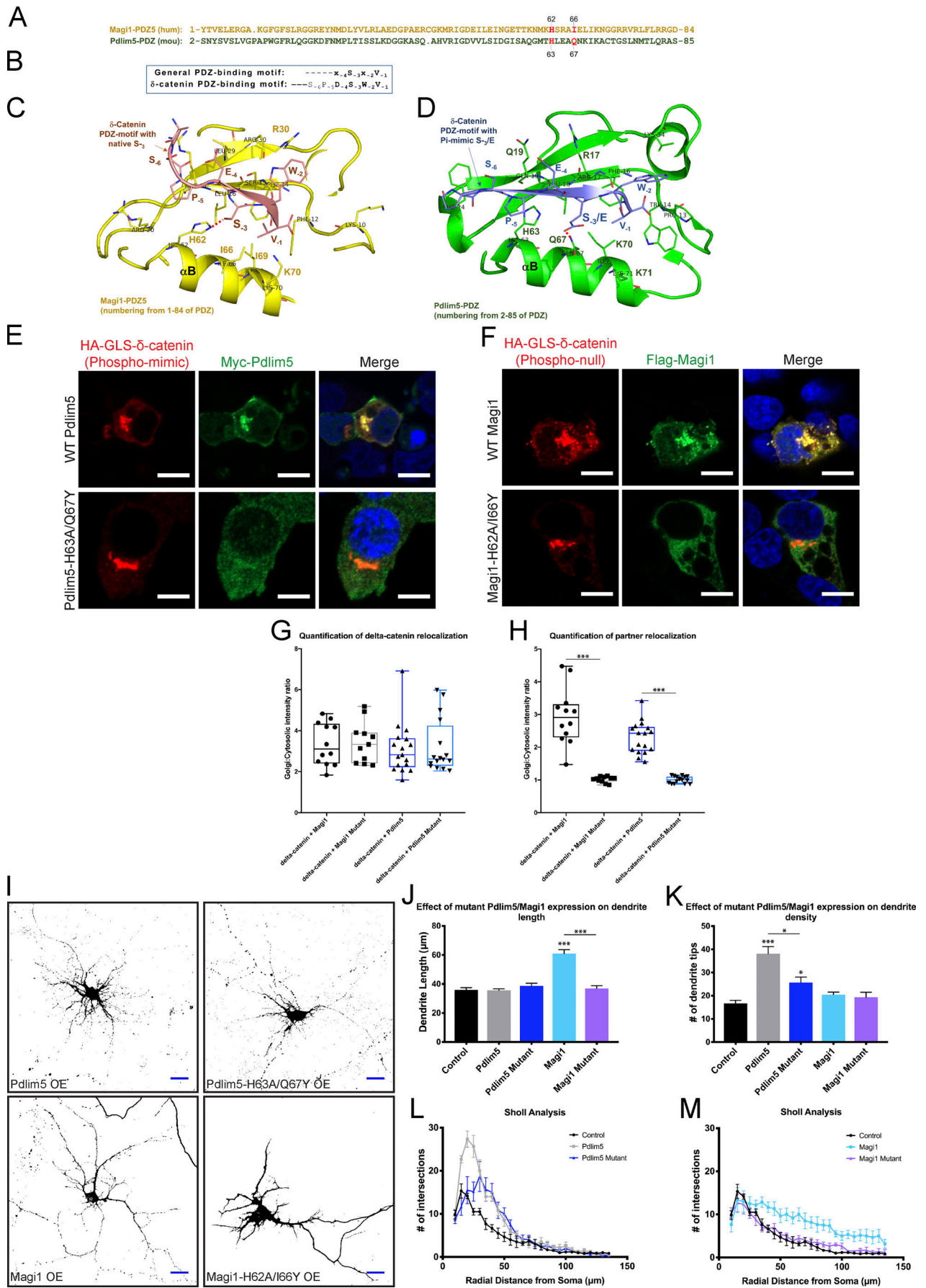


Figure 8. Influence of Magi1 and Pdlim5 on dendrite development weakens in absence of interaction with delta-catenin. (A) Amino protein sequences of human Magi1 PDZ5 and mouse Pdlim5 PDZ. Residues mutated to prevent interaction with delta-catenin are highlighted in red (Magi1: H62A/I66Y; Pdlim5: H63A/Q67Y). (B) Amino acid schematic of a general PDZ-binding motif and delta-catenin's PDZ binding motif, showing serines at -3 and -6 locations. (C and D) Models of the Magi1:delta-catenin (C) and Pdlim5:delta-catenin (D) interactions. (E and F) Validation of lack of interaction between mutant Pdlim5 and Magi1 with delta-catenin via a GRA in HEK293 cells. (G) Quantification of delta-catenin localization in GRA. (H) Quantification of Magi1/Pdlim5 localization in GRA. Graphs represent cultures from at least two independent experiments. (I) Representative images of 7-DIV primary rat hippocampal neurons expressing Pdlim5 cDNA, Pdlim5-H63A/Q67Y cDNA, Magi1 cDNA, and Magi1-H62A/I66Y cDNA. (J) Quantification of average dendrite length of neurons expressing GFP ($35.96 \pm 1.56 \mu\text{m}$), Pdlim5 cDNA ($35.69 \pm 1.01 \mu\text{m}$; $P = 0.9916$), Pdlim5-H63A/Q67Y cDNA ($38.63 \pm 1.85 \mu\text{m}$; $P = 0.873$), Magi1 cDNA ($60.98 \pm 2.69 \mu\text{m}$; $P < 0.0001$), and Magi1-H62A/I66Y cDNA ($36.97 \pm 1.86 \mu\text{m}$; $P = 0.997$). Overexpression of Magi1-H62A/I66Y failed to induce the dendrite extension that results from native Magi1 overexpression ($P \leq 0.0001$). (K) Average dendrite density of neurons expressing GFP (16.69 ± 1.26), Pdlim5 cDNA (38.13 ± 3.06 ; $P < 0.0001$), Pdlim5-H63A/Q67Y cDNA (25.70 ± 2.32 ; $P = 0.0491$), Magi1 cDNA (20.50 ± 1.04 ; $P = 0.0690$), and Magi1-H62A/I66Y cDNA (19.4 ± 2.06 ; $P = 0.914$). Neurons overexpressing Pdlim5-H63A/Q67Y failed to increase dendrite density to the extent of native Pdlim5 overexpression ($P = 0.0016$). (L) Sholl analysis of dendrite morphology for GFP control, Pdlim5-overexpressing, and Pdlim5 mutant (H63A/Q67Y)-overexpressing neurons. Relative to GFP-expressing cells, neurons overexpressing Pdlim5-H63A/Q67Y possessed significantly more dendrites at $40 \mu\text{m}$ ($P = 0.0315$) and $50 \mu\text{m}$ from the soma ($P = 0.0333$). Relative to neurons overexpressing native Pdlim5, neurons overexpressing Pdlim5-H63A/Q67Y developed significantly fewer dendrites at $15\text{--}25 \mu\text{m}$ from the soma ($P < 0.05$). (M) Sholl analysis of dendrite morphology for GFP control, Magi1-overexpressing, and Magi1 mutant (H62A/I66Y)-overexpressing neurons. Relative to overexpression of native Magi1, neurons overexpressing Magi1-H62A/I66Y possessed significantly fewer dendrites at $40 \mu\text{m}$ ($P = 0.0090$) and $60 \mu\text{m}$ from the soma ($P = 0.0357$). Overexpression of Magi1-H62A/I66Y produced no changes in dendrite length/density relative to GFP controls. *, $P < 0.05$; ***, $P \leq 0.0001$. For G and H, box plots indicate upper and lower quartiles (top/bottom of box), median value (center line of box), and the maximum/minimum values (whiskers). For J–M, error bars indicate SEM. For all conditions in I–K, $n \geq 12$ neurons; in L and M, $n = 6$. For G, H, J, and K, significance was determined using a one-way ANOVA followed by Tukey's test. For L and M, a two-way ANOVA with Bonferroni post-hoc analysis was used. For E and F, scale bars, $10 \mu\text{m}$. For I, scale bars, $20 \mu\text{m}$. OE, overexpression.

conditions (Buard et al., 2010; Procko and Shaham, 2010). There is also existing evidence of glial glutamate release and uptake modulating synaptic activity and dendritic spine morphology (Angulo et al., 2004; Verbich et al., 2012). This raises the question of whether glial cells surrounding neurons are providing dendritic growth cues via the regulation of local glutamate levels. However, there is evidence that glia-induced dendritic branching occurs via glutamate-independent mechanisms as well, such as via the secretion of phosphatidic acid, Semaphorin, Netrin, and certain Slit family members (Polleux et al., 2000; Godenschwege et al., 2002; Furrer et al., 2003; Kim and Chiba, 2004; Zhu et al., 2016). A second possibility is a neuronal source of glutamate. Recent evidence suggests that spontaneous axonal release of extrasynaptic glutamate plays a significant role in establishing the complexity of the dendritic arbor, though whether axonal glutamate activates type 1 mGluR receptors along dendrites in this context remains unknown (Andreae and Burrone, 2015). While the source of the glutamate responsible for instructing neuronal development remains debated, our findings reveal novel mechanisms that underlie glutamate's role in dendrite development and link these mechanisms to morphological changes in the dendritic arbor. In the future, it will be interesting to further elucidate how upstream external and/or intrinsic cues converge and participate in pathways that instruct dendrite morphology.

Downstream effectors of delta-catenin phosphorylation in dendrite development

Given that the elaboration of dendritic arborizations is largely dependent on cytoskeletal remodeling, it is likely that the mGluR5 signaling-induced phosphorylation of delta-catenin and its subsequent associations with Magi1 or Pdlim5 lead in part to the modulation of proteins underlying actin or microtubule dynamics in dendrites. The Rho family of small GTPases has extensive roles in neurite development and maintenance via cytoskeletal remodeling (Govek et al., 2005). RhoA activity inhibits dendritic branching in hippocampal neurons, with a

recent study involving a G protein-coupled receptor (BAII) reporting that dendritic RhoA activity normally increases in later stages of dendrite growth as a means to terminate arborization (Nakayama et al., 2000; Duman et al., 2019). Conversely, delta-catenin has been reported to inhibit RhoA activity via the sequestration of a RhoA activator (p190RhoGEF), enhancing dendrite arborization and growth (Kim et al., 2008a). In addition to RhoA, two other Rho family members, Rac1 and Cdc42, have also been implicated in dendritic formation and elaboration (Threadgill et al., 1997; Vadodaria et al., 2013). Both Rac1 and Cdc42 have been shown to be activated in response to type 1 mGluR stimulation via DHPG treatment, as well as delta-catenin overexpression, in hippocampal neurons (Abu-Elneel et al., 2008). However, some groups have reported no change in the activity of either GTPase in response to delta-catenin expression levels, suggesting that delta-catenin's impact on dendritic morphology may not be dependent on global activation of Rac1 and Cdc42, but rather modulation of these proteins in microenvironments along the length of growing dendrites (Arikkath et al., 2008; Kim et al., 2008a).

Previous studies have found that delta-catenin's inhibition of RhoA activity is dependent on the phosphorylation of Thr-454 and subsequent interaction with p190RhoGEF (Kim et al., 2008a). There is also evidence that loss of delta-catenin may not necessarily affect total levels of active RhoA in neurons, as is the case for Rac1 and Cdc42 (Arikkath et al., 2008). Collectively, as alluded to above, and in consideration of the relatively small fraction of phosphorylated delta-catenin present in neurons, these findings suggest that delta-catenin's modulation of Rho-family GTPase activity may depend on micro-environmental factors—distributed unevenly even within single cells—that promote versus constrain phosphorylation of delta-catenin's PDZ-binding motif in specific dendritic regions. While we observe total cellular decreases of RhoA activity in HEK293 cells that exogenously express a phospho-mimic delta-catenin that promotes its interaction with Pdlim5 (which promotes dendritic

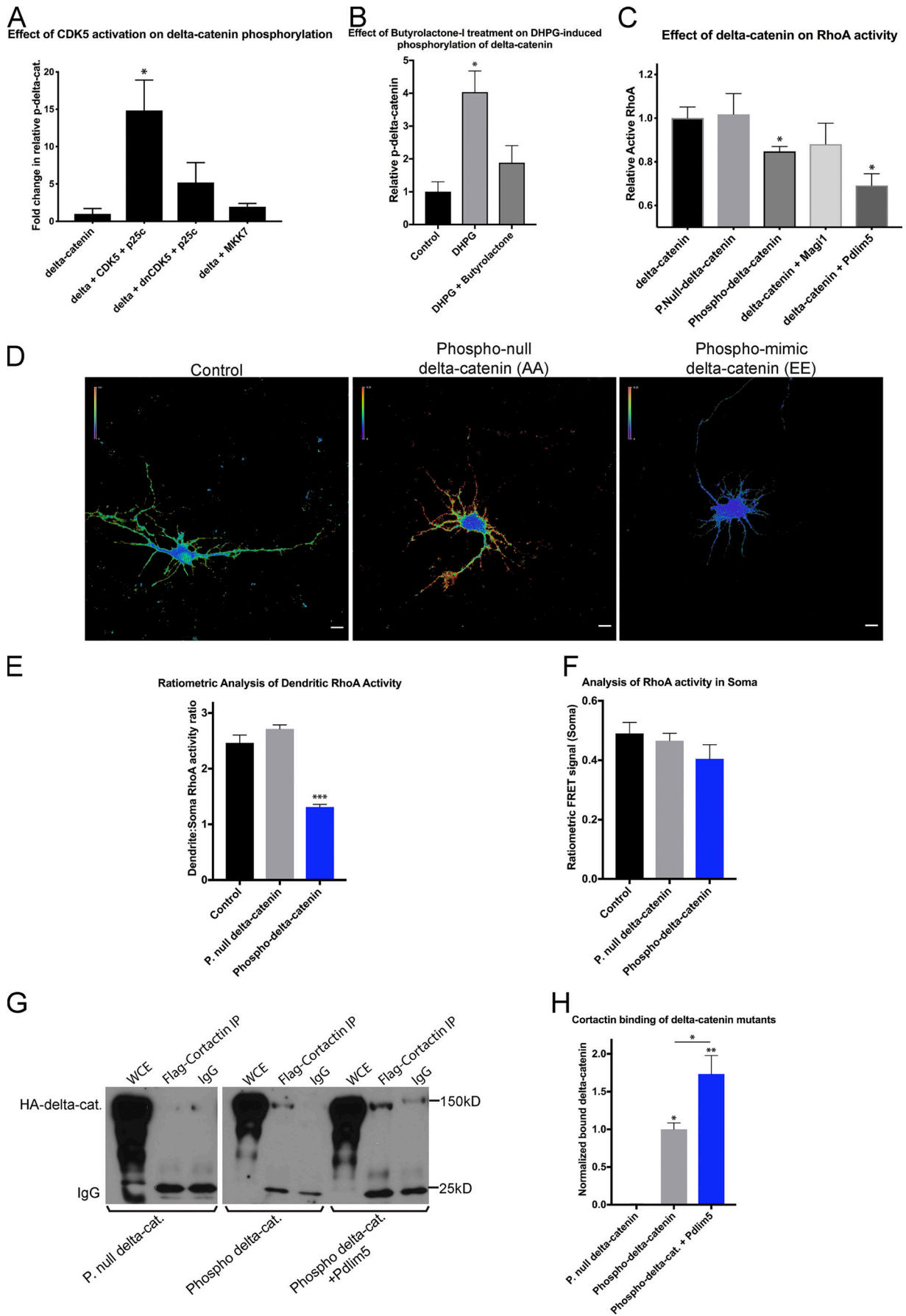


Figure 9. **Identification of the modulatory kinase and downstream effectors associated with phosphorylation of delta-catenin's PDZ-binding motif.**

(A) Representation of fold change in levels of phosphorylated delta-catenin relative to total delta-catenin in response to exogenous coexpression of the indicated kinases in HEK293 cells. Coexpression of constitutively active CDK5 and p25c with delta-catenin resulted in a 15-fold increase in the relative amount of phosphorylated delta-catenin in cell lysates ($P = 0.0113$); $n = 3$ independent cultures/experiments. **(B)** Quantification of fold change in relative levels of phosphorylated delta-catenin in primary rat hippocampal neurons (7 DIV) following DHPG treatment with and without pretreatment with Butyrolactone I. Pretreatment of cultures with Butyrolactone I largely prevented the DHPG-induced increase ($P = 0.0404$) in delta-catenin phosphorylation levels relative to controls ($P = 0.5205$); $n = 3$ independent cultures/experiments. **(C)** Quantification of levels of active RhoA in HEK293 cells expressing WT delta-catenin (baseline), phospho-null delta-catenin (102% of baseline; $P = 0.8814$), phospho-mimic delta-catenin (85% of baseline; $P = 0.0332$), Magi1 + delta-catenin (88% of baseline; $P = 0.3152$), or Pdlim5 + delta-catenin (69% of baseline; $P = 0.0059$); $n = 4$ independent experiments. **(D)** Representative ratiometric FRET confocal images of 4-DIV primary rat hippocampal neurons expressing a FRET-based (CFP-YFP) RhoA biosensor in combination with phospho-null or phospho-mimic delta-catenin mutants. **(E)** Quantification of ratio of dendrite-to-soma RhoA activity (Fr) in biosensor-expressing neurons, as observed via ratiometric FRET. Relative to controls (Fr = 2.462 ± 0.142), expression of phospho-null delta-catenin produced no change in dendritic RhoA activity (Fr = 2.713 ± 0.074 ; $P = 0.2098$). Expression of phospho-mimic delta-catenin produced a significant decrease in dendritic RhoA activity (Fr = 1.312 ± 0.048) compared with both control ($P < 0.0001$) and phospho-null delta-catenin -expressing neurons ($P < 0.0001$). **(F)** Quantification of RhoA activity in the soma of biosensor-expressing neurons, as observed via ratiometric FRET. Expression of either phospho-null or phospho-mimic delta-catenin in primary rat hippocampal neurons produced no changes in RhoA activity in the soma of neurons ($P = 0.8906$; $P = 0.2903$). For D–F, $n = 4$ neurons from independent cultures. **(G)** Immunoblot of HA-delta-catenin coimmunoprecipitation with Flag-Cortactin from HEK293 cell lysates. IP, immunoprecipitation. WCE, whole cell extract. **(H)** Densitometric quantification (normalized to total delta-catenin and antibody) of relative (to phospho-mimic) amounts of delta-catenin mutants pulled down by Cortactin. Phospho-null delta-catenin failed to coimmunoprecipitate with Cortactin, while phospho-mimic delta-catenin successfully immunoprecipitated with Cortactin ($P = 0.0077$). This association was further stabilized by coexpression of Pdlim5 ($P = 0.0301$). For H, $n = 3$ independent cultures/experiments. *, $P < 0.05$; **, $P \leq 0.001$; ***, $P \leq 0.0001$. For A–C, E, F, and H, significance was determined using a one-way ANOVA followed by Tukey's test. Error bars indicate SEM. Scale bars, 10 μm .

branching, as does delta-catenin and Pdlim5 coexpression), we envisage that phosphorylation of endogenous delta-catenin at its –6 and/or –3 serines normally occurs in defined dendritic (or other) regions as opposed to across the entire internal volume of the neuron, and thus that the total cellular levels of RhoA activity remain largely unaltered. Indeed, utilization of FRET-based RhoA biosensors in neurons overexpressing phospho-mimic versus phospho-null delta-catenin mutants revealed a decrease in RhoA activity strictly in the dendrites of neurons expressing the phospho-mimic mutant. Therefore, we propose that localized sub-dendritic regions of increased RhoA inhibition arise upon similarly localized delta:Pdlim5 complex association (e.g., following delta-catenin's –6 and –3 serine phosphorylation), relating to the promotion of dendritic branching or the stabilization of branches at these loci. Further, the data support that delta-catenin's ability to modulate Rho-family small GTPases, and/or other regulators of the cytoskeleton, is linked to delta-catenin's phosphorylation state and consequent interactions (versus not) with Magi1 or Pdlim5.

While our findings, as well as previous studies, suggest that small GTPases are relevant to delta-catenin's functions, delta-catenin has also been found to promote neurite elongation and branching upon the phosphorylation-dependent binding of Cortactin, an actin-associated protein that induces actin nucleation through association with the Arp2/3 complex (Martinez et al., 2003). Expression of delta-catenin mutants unable to bind Cortactin fail to induce the dendrite-like processes characteristic of wild-type delta-catenin overexpression in PC12 cells (Martinez et al., 2003). Here, we reveal that the delta-catenin:Cortactin complex preferentially forms when delta-catenin's PDZ-binding motif is phosphorylated, and that this association is favored in the presence Pdlim5. Given the absence of a PDZ domain in Cortactin, and as Pdlim5 is a PDZ protein that binds the phosphorylated PDZ-binding motif of delta-catenin, Pdlim5 could be well positioned to assist in facilitating or stabilizing the delta:Cortactin interaction. Cortactin has been shown to dynamically localize to sites of actin assembly, leading to the possibility that phosphorylated delta-catenin may recruit/stabilize Cortactin to

future dendritic branch points to promote actin assembly and ultimately the formation of an extending branch (Weed et al., 2000). This recruitment may be further facilitated by Pdlim5, which is known to associate with the actin cytoskeleton via an interaction with α -actinin (Lasorella and Iavarone, 2006). Thus, the delta:Magi1 and delta:Pdlim5 complexes, and the subsequent small-GTPase modulation suggested here, may function in parallel with actin nucleation events initiated by the (phosphorylated) delta-catenin:Cortactin:Pdlim5 complex at sites of elevated metabotropic glutamate signaling to dynamically mediate branching versus neurite elongation during dendrite morphogenesis. To further elucidate their underlying mechanisms, future study will be required to investigate the relationships between the delta:Magi1 and delta:Pdlim5 complexes and other delta-catenin-associated proteins relevant to cytoskeletal function. In all cases, our findings indicate novel roles for Magi1 and Pdlim5 in contributing to the modulation of small GTPases and the Cortactin:Arp2/3 complex, all potent actin regulators, in dendrite development by delta-catenin.

Further, as would be anticipated, there are prior examples of catenin functions requiring an interaction with partner proteins reading defined catenin phosphorylation states (Gottardi and Gumbiner, 2004; Gu et al., 2011; Hong et al., 2016; Nusse and Clevers, 2017). We note also that the “phospho-switch” mechanism we have revealed within the PDZ-binding motif of delta-catenin may extend to certain additional catenin proteins. For example, p0071-catenin possesses a nearly identical PDZ-binding motif inclusive of the noted –6 and –3 serine residues (Izawa et al., 2002). Thus, we view it as probable that the further elucidation of delta-catenin's phospho-switch and its downstream effectors will shed light upon the function of additional catenins in cell/tissue types beyond neurons.

Magi1, Pdlim5, and other PDZ proteins in dendrite development

PDZ domain-containing proteins have multiple roles in many aspects of neuronal development. For instance, PSD-95, a member

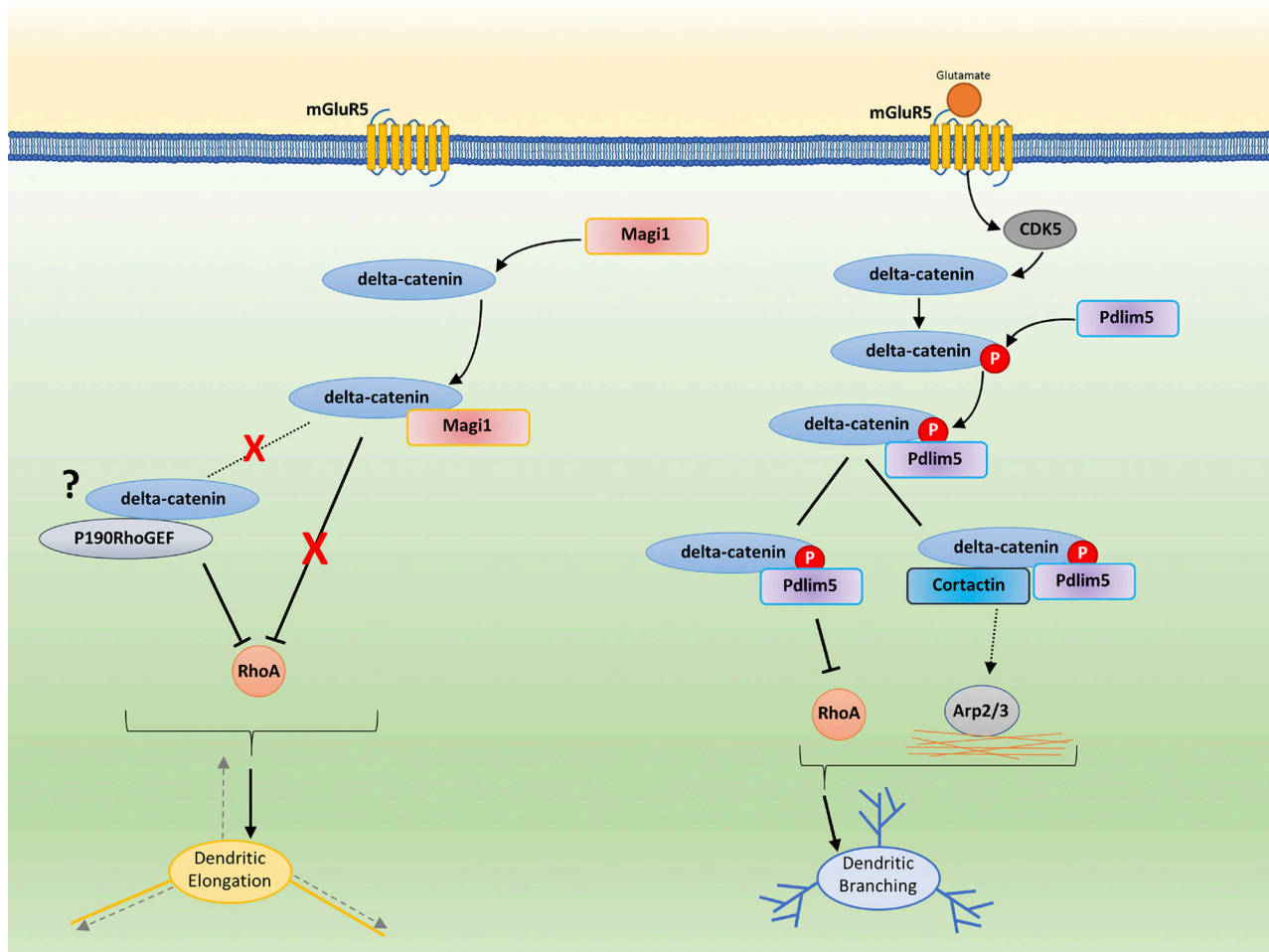


Figure 10. Proposed model of delta-catenin signaling during dendrite development. In the absence of glutamate signaling (left side of schematic), delta-catenin remains unphosphorylated within its PDZ-binding motif (–6 and –3 serines counting back from delta’s C-terminal valine). This allows delta-catenin to bind Magi1, disrupting delta-catenin’s indirect inhibition of RhoA activity. Speculatively in this regard, Magi1 might make delta-catenin less apt to sequester RhoA activators such as p190RhoGEF (which is known to associate with delta-catenin), lessening RhoA inhibition (relative to delta:Pdlim5 association), and ultimately promoting dendrite elongation. Conversely, in response to glutamate signaling and type 1 mGluR activation (right side of schematic), delta-catenin is phosphorylated by CDK5 within its PDZ-binding motif (–6 and likely –3 serines). Such PDZ-binding motif phosphorylation prevents the binding of Magi1. Instead, delta-catenin binds Pdlim5, which enhances delta-catenin’s inhibition of RhoA activity to a greater extent (than delta:Magi1), and which promotes the delta:Cortactin interaction, to further local actin polymerization and dendritic branching. P, phospho/phosphorylated.

of the MAGUK family of proteins, stabilizes AMPA receptors in the postsynaptic density via interactions with Stargazin and other auxiliary proteins in complex with these receptors (Schnell et al., 2002; Chen et al., 2015). Another synaptic PDZ domain-containing MAGUK family member, Magi2 (also known as synaptic scaffolding molecule, or S-SCAM), acts as a scaffolding molecule for GluA2-containing AMPA receptors and is believed to play a role in synaptic plasticity (Danielson et al., 2012). Interestingly, both PSD-95 and Magi2, like Magi1, also interact with the PDZ-binding motif of delta-catenin (Ide et al., 1999; Silverman et al., 2007). Our preliminary findings suggest that like Magi1, PSD-95 and Magi2 interact only with the unphosphorylated PDZ-binding motif of delta-catenin (PSD-95 data not shown). Given the known roles of MAGUK members in neural development, several may function via associations with delta-catenin, in a similar fashion to Magi1, in regions outside of the dendrite. Accordingly, further research is needed upon

MAGUK proteins in neural development, inclusive of the impact of delta-catenin’s phosphorylation in morphogenesis.

Our findings on Magi1 and Pdlim5 indicate that these two proteins have opposing roles in the context of hippocampal neuron dendrite development. Magi1 promotes dendritic elongation in developing hippocampal neurons. Exogenous Magi1 expression greatly increases dendrite length, while the number of dendritic branches appears largely unaffected. Magi1 shRNA-mediated KD correspondingly results in neurons with shorter dendrites. Pdlim5, conversely, promotes dendrite branching while simultaneously restricting dendrite growth in hippocampal neurons. We found that hippocampal neurons overexpressing Pdlim5 develop significantly more dendrites. Unexpectedly but suggesting some crosstalk, neurons partially knocked down for Pdlim5 did not exhibit reduced dendritic branching, but instead showed increased dendrite length.

The reduced functional impact of Magi1 or Pdlim5 on dendrite morphology when expressing point mutants that are incapable of binding delta-catenin suggests that the dendritic roles of these proteins may be dependent on their respective associations with delta-catenin. Accordingly, the dendritic functions of Magi1 and Pdlim5 are likely intertwined with delta-catenin's regulation of small GTPase activity. Our data suggest that Pdlim5's phosphorylation-dependent association with delta-catenin acts to enhance the inhibition of RhoA activity while concurrently stabilizing the delta:Cortactin interaction. This complex may then promote actin assembly via the Cortactin:Arp2/3 complex interaction in an environment of reduced RhoA activity, leading to the formation of a dendritic branch. In the absence of glutamate signaling, Magi1's association with delta-catenin does not decrease RhoA activity or appear to allow for delta-catenin's association with Cortactin. A potential explanation for these observations is that, in the tips of growing dendrites, where Magi1 is most highly localized, unphosphorylated delta-catenin is sequestered or prevented by Magi1 from interacting with certain GTPase regulatory proteins, such as p190RhoGEF (Kim et al., 2008a), or actin-associated proteins, including Cortactin. This would prevent the formation of new branches and possibly instead facilitate delta-catenin's association with other known interaction partners involved in neurite outgrowth, such as N-cadherin, or with Cortactin-independent actin regulatory complexes (Neugebauer et al., 1988). Our preliminary findings (data not shown) suggest, however, that delta-catenin's binding to Magi1 versus Pdlim5 does not affect the association of delta-catenin with N-cadherin, though the potential for stabilization of N-cadherin at the membrane of dendritic tips by delta-catenin, facilitated by Magi1, remains a possibility.

To summarize, the results from this study provide mechanistic insight into the intrinsic changes elicited by a glutamate and CDK5-kinase signaling trajectory during early neuron development. Our findings implicate delta-catenin in a novel phosphorylation-dependent pathway defining dendrite morphology in hippocampal neurons. This occurs through delta-catenin's interactions with Magi1 versus Pdlim5. We provide evidence that delta-catenin's "phospho-switch" operates downstream of mGluR5 activation during dendrite development, enabling decisions of elongation versus branching wherein the differential regulation of RhoA and Cortactin could be involved in localized cytoskeletal modulation. While this report focuses upon the delta:Magi1 versus delta:Pdlim5 complexes, we note that phosphorylation of delta-catenin's PDZ-binding motif is likely to affect additional PDZ-domain interactions. This would expand the relevance of delta-catenin's newly revealed phospho-switch beyond what is already a strong indicator here, where two novel delta-catenin interactions are shown to promote dendrite lengthening versus branching morphologies.

Materials and methods

Cell culture and transfections

Cell culture and transfection of HEK293 cells

HEK293 cells were purchased from ATCC and maintained in DMEM cell culture media (Sigma-Aldrich) supplemented with

10% FBS (Sigma-Aldrich) and 1× penicillin-streptomycin (Life Technologies). Culture media was changed every other day until cells reached 80% confluency, at which point they were passaged into a new culture dish/plate. HEK293 cells were transfected using Lipofectamine 3000 and the manufacturer's recommended protocol. Cells were transfected at 50–60% confluency per well in a six-well culture plate. For Golgi co-relocalization, cells were fixed and imaged 24 h after transfection and examined via confocal microscopy. For shRNA-mediated KD and immunoprecipitation analyses, cells were lysed 24–48 h after transfection and immunoblotted, as described below.

Cell culture and transfection of neurons

Primary hippocampal neurons were isolated from rat embryos (E18) as previously described (Fischer et al., 2018). Briefly, hippocampal neurons were plated in 24-well tissue-culture plates (2×10^5 /well), containing glass coverslips coated with 100 μ g/ml poly-D-lysine (Sigma-Aldrich). The hippocampal cultures were maintained in Neurobasal Medium (Life Technologies) supplemented with B-27 (Life Technologies), GlutaMAX (Life Technologies), and penicillin-streptomycin (Life Technologies). At 3 DIV, neurons were transfected using Lipofectamine 3000 with 1 μ g of plasmid DNA and a modified manufacturer's protocol (Life Technologies). All cDNA transfections for overexpression analyses used cDNA in the pCS2 expression vector. All shRNA-mediated KDs used the pSUPER shRNA expression vector (Oligoengine). For pharmacological treatments, DHPG was purchased from Cayman Chemical (14411), while Butyrolactone I (203988) and MTEP (445874) were purchased from Sigma-Aldrich.

DNA/RNA construct synthesis and validation

DNA constructs

All DNA constructs were cloned into the pCS2 mammalian expression vector by the McCreary Laboratory. All truncations, deletions, and site mutations were generated via PCR and confirmed with DNA sequencing. The full-length delta-catenin construct contains an N-terminal HA epitope tag and a stop codon immediately following the C-terminal of delta-catenin to best preserve the function of the C-terminal PDZ-binding motif. This delta-catenin construct was used as the backbone for the delta-catenin-AA (phospho-null) and delta-catenin-EE (phospho-mimic) constructs. All Magi1 constructs in this study use a pCS2-FLAG vector, while the Pdlim5 constructs use a pCS2-Myc vector. All kinase constructs used (dnCDK5, CDK5, p25C, and MKK7) used the pcDNA3-GFP expression vector and were kind gifts from Jeff Frost (University of Texas Health Science Center at Houston [UTHealth], Houston, TX).

shRNA synthesis and validation

The Oligoengine pSUPER-GFP and pSUPER-mOrange shRNA vectors were used as the backbone for all shRNA constructs used in this study. For Magi1 and Pdlim5 shRNA, target sequences 19 nucleotides in length were identified via the siRNA Wizard v3.1 tool (InvivoGen) and used to generate the hairpin RNA. All Magi1 and Pdlim5 shRNA sequences were purchased from GE Dharmacon, then annealed and inserted into the pSUPER-GFP

vector following the manufacturer's protocol (Oligoengine). The delta-catenin shRNA (pSUPER-mOrange) was a kind gift from Jyothi Arikath (University of Nebraska, Lincoln, NE) and has been validated and published on several occasions (Arikath et al., 2008, 2009). All construct sequences were validated via the DNA sequencing facility at MDACC. The sequences for the shRNA targeting each protein are as follows: Delta-catenin: 5'-TAGAAGTCGACATAGTTGC-3'; Magi1: 5'-GGAATGTGATACGTG TCTA-3'; Pdlim5: 5'-GCACTGTATTGTGAGCTAT-3'.

KD efficiency of each shRNA was validated via transient transfection of HEK293 cells expressing either HA-delta-catenin, FLAG-Magi1, or Myc-Pdlim5 with the respective shRNA construct. The neuronal phenotypes produced by shRNA KD of Pdlim5 and Magi1 were validated via exogenous rescue with epitope-tagged Magi1/Pdlim5 (Fig. S3, B-H). Cells were allowed to grow for 24–48 h before subjecting the cell lysates to immunoblot analysis. Immunoblots were quantified using densitometry (ImageJ) to calculate a general KD efficiency percentage for each shRNA (Fig. S3 A). We noticed a near-complete loss of delta-catenin protein levels in HEK293 cells transfected with shRNA. Both Magi1 and Pdlim5 exhibited partial KD, with a ~68% loss of Magi1 and ~60% loss of Pdlim5 in shRNA-expressing cultures. While it will be interesting to achieve a more complete KD of Magi1 and Pdlim5, we found that even a partial KD of either protein in hippocampal neurons is sufficient to generate morphological changes (Fig. 7).

Biochemical/immunofluorescent analysis

GRA

To visualize protein–protein interactions with higher sensitivity and reproducibility than with techniques relying on cell lysis, the McCrea laboratory developed a novel protein co-relocalization assay (GRA), in which a single protein (delta-catenin) is redirected to the Golgi apparatus, causing any interaction partners of the protein to also relocalize to the Golgi. Since GRA avoids detergent lysis and wash conditions involved in coimmunoprecipitations, weaker or transient interactions have a higher probability of being detected. To relocalize delta-catenin to the Golgi, we synthesized a fusion protein consisting of full-length delta-catenin with the Golgi localization sequence (GLS) from mammalian target of rapamycin (mTOR) fused to the protein's N-terminus. The reason for using this particular sequence is that it remains functional at both the N-terminus and C-terminus of most proteins, unlike many other organelle localization sequences. Following transfection, cells were subjected to a standard immunofluorescence staining protocol and were qualitatively analyzed for relocalization of potential partner proteins to the Golgi with delta-catenin + GLS. Quantitative analysis was accomplished by comparing the average fluorescence intensity of the Golgi body to that of the cytosol for each channel to generate a Golgi:cytosolic intensity ratio for each channel/condition. The ImageJ software was used for ROI selection and intensity measurements.

GLS from mammalian target of rapamycin: 5'-ACTAGTGAA ATGCTGGTCAACATGGGAACTTGCCTCTGGATGAGTTCTAC CCAGCTGTGTCCATGGTGGCCCTGATGCGGATCTTCCGA GACCAGTCACTCTCTCATCATCACACCATGTTGTCCAG

GCCATCACCTTCATCTTCAAGTCCCTGGGACTCAAATGTGTG CAGTTCCTGCCCCAGGTGATGCCACGTTCTTAACGTCATT CGAGTCTGTGATGGGGCCATCCGGGAATTTTGTTCAGCAG CTGGGAATGTTGGTGTCTTTGTGAAGAGCCACATCAGACCT TATATGGATGAAATAGTCCACCTCATGAGA-3'.

Detection and quantification of phosphorylated delta-catenin

Phosphorylation of delta-catenin's PDZ-binding motif was detected through the use of a commercial monoclonal rabbit antibody (Cell Signaling Technologies) directed against an established phospho-MAPK/CDK consensus (PXS*P) that we observed within the PDZ-binding motif of delta-catenin (Contreras-Vallejos et al., 2014; Morey et al., 2015; Urizar-Arenaza et al., 2019). The consensus serine is present at the –6 residue position counting from delta-catenin's terminal valine (YPASPDSWV). When used in combination with a separate established monoclonal delta-catenin-specific antibody (BD Technologies; Arikath et al., 2008; Yuan et al., 2015), we were able to quantify the relative amount of phosphorylation at the –6 serine position within delta-catenin's PDZ-binding motif. Specifically, cell lysates were first subjected to immunoprecipitation using the Cell Signaling Technologies PXS*P antibody (catalog # 2325S), which detects serine phosphorylation events within this consensus. The resulting IP samples (which contain phospho-delta-catenin, among other phosphorylated proteins) were subsequently subjected to immunoblot analysis, where delta-catenin was specifically resolved with a monoclonal antibody directed against delta-catenin (BD Technologies, catalog # 611537), allowing for the detection of delta-catenin phosphorylated within its PDZ-binding motif (PXS*P). We validated the specificity of the p-MAPK/CDK antibody to the –6 serine position within delta-catenin by expressing wild-type versus phospho-null constructs of delta-catenin in HEK293 cells, followed by immunoblotting (Fig. 4 A). We detected phosphorylation in exogenously expressed wild-type delta-catenin, but not in the phospho-null point mutant where the –6 and –3 serines had been mutated to alanine. This suggests that the anti-MAPK/CDK consensus antibody, when combined with the delta-catenin-specific antibody, reports upon the relative phosphorylation levels of delta's PDZ-binding motif.

RhoA activity assay

For RhoA activity quantification, the RhoA G-LISA kit from Cytoskeleton, Inc. was used. For this solid phase ELISA-based assay, the manufacturer's protocol was followed. Briefly, HEK293 cells were cultured and transfected as described above. 24 h after transfection, cells were lysed and subjected to an active RhoA-specific luminescence-based ELISA. Relative luminescence was measured with a FLUOstar Omega Microplate Reader (BMG Labtech) and normalized to blanks (lysis buffer alone) and compared with controls (untransfected HEK293 cells).

PLA

For the PLA, cells (either HEK293 or primary hippocampal neurons) were cultured and maintained as described above. For neuronal PLA, cells were fixed at 7 DIV. For HEK293 PLA, cells

were transfected then fixed 24 h after transfection, as described above. The PLA kit used was manufactured by Duolink (now part of Sigma-Aldrich) and purchased from Sigma-Aldrich. The manufacturer's protocol was followed during this assay. Briefly, cells were permeabilized, blocked, and incubated with primary antibodies, similar to our protocol for immunofluorescence staining. Following primary antibody incubation, the cells were washed with PBS and incubated with Duolink PLA probes, which recognize the primary antibodies, before being incubated with a ligase and amplification enzymes to generate the DNA structure that is recognized by provided fluorescent probes. Finally, cells were incubated with said fluorescent probes and imaged using a Nikon T2i Inverted Confocal Microscope with an Apo-Plan 60× 1.4 NA oil objective at a pixel size of 100 nm. Stacks were converted to maximum projection images for analysis. Puncta were quantified using the Puncta Analyzer plugin for the ImageJ software.

Coimmunoprecipitation and immunoblots

For immunoblotting assays, cells were cultured, maintained, and transfected as described above. For HEK293 cells, cells were lysed 24–48 h after transfection. For neuronal cultures, cells were lysed at 7 DIV. For coimmunoprecipitation, an established and familiar protocol was followed. Following lysis, protein concentrations of cell lysates were equalized and incubated with primary antibodies in 1.5-ml conical tubes for 1 h at 4°C while rotating. After 1 h, A/G agarose (Santa Cruz Biotechnologies) beads were added to each tube and incubated for an additional 1 h at 4°C while rotating. Following this secondary incubation, protein was eluted from beads through the addition of 2× sample buffer with βME and heated at 95°C for 5 min. Eluted immunoprecipitation samples, and in the case of immunoblots, equalized cell lysates, were then loaded into an 8% acrylamide gel and run for 120 min. Proteins were then transferred to nitrocellulose membranes (GE Whatman) using a Pierce Power Blotter (Thermo Fisher Scientific). Resulting protein-loaded membranes were then blocked in a TBS with Tween 20 + 1% dry milk solution overnight at 4°C. Blocked membranes were incubated in primary antibodies overnight at 4°C before being incubated in HRP-conjugated secondary antibodies (Invitrogen). Lastly, membranes were incubated with SuperSignal West luminol solution (Thermo Fisher Scientific) and imaged using autoradiography film and a X-OMAT Developer.

Confocal microscopy/STORM imaging

Immunofluorescence staining

Immunostaining of HEK293 and primary hippocampal neurons was completed using an established protocol (Lee et al., 2014). Briefly, cells cultured on poly-D-lysine-coated coverslips were fixed with 4% paraformaldehyde for 10 min at room temperature and then permeabilized with 0.5% Triton X-100 solution for 15 min. Following fixation and permeabilization, cells were blocked with PBS containing 1% bovine serum albumin overnight at 4°C. After blocking overnight, cells were incubated with indicated primary antibodies overnight at 4°C and then rinsed three times with fresh PBS for 10 min each, followed by an overnight rinse with PBS at 4°C. Cells were then incubated with

Alexa Fluor fluorescent dye-conjugated secondary antibodies (Invitrogen) for 1 h at room temperature before the coverslips were finally mounted onto glass slides with Vectashield (Vector Laboratories) mounting solution. Cells were visualized using a Nikon T2i Inverted Confocal Microscope with an Apo-Plan 60× 1.4 NA oil objective at room temperature. Images were captured with a Nikon A1-DUG GaAsP hybrid four-channel multi-detector and Nikon NIS-Elements software. All z-series images were acquired at a pixel size of 100 nm and a step size of 0.2 μm.

STORM imaging

For super-resolution imaging, the manufacturer's protocol was followed (Nikon). Briefly, primary hippocampal neurons were isolated, as previously described, and plated onto 35-mm Mat-Tek dishes coated with poly-D-lysine. Cells were fixed for 10 min at room temperature with 4% paraformaldehyde and permeabilized with 0.5% Triton X-100 solution for 15 min. The cells were then blocked with PBS containing 1% bovine serum albumin for 90 min at room temperature before incubating overnight at 4°C in primary antibodies. The cells were then washed five times with PBS for 15 min each (75 min total), followed by an incubation with secondary antibodies (Atto 488 and Alexa Fluor 647) for 1 h at room temperature. Lastly, the cells were washed another five times with PBS for 15 min each (75 min total) and finally fixed a second time with 4% paraformaldehyde (no shaking) for 10 min. The cells were then rinsed with PBS three times, for 5 min per rinse, and stored in distilled H₂O until ready to image. Cells were never stored for longer than 24 h at 4°C after preparation. For imaging, distilled H₂O was replaced with a STORM Imaging Buffer with monoethanolamine, as described in the manufacturer's protocol (Nikon N-STORM). Images were acquired using an APO-Plan TIRF 100× 1.49 NA objective and STORM 3D lenses. Laser lines 488 nm and 647 nm were used for excitation of the sample, and emission was collected with a Quad C161417 TIRF filter set with band pass emitters at 525/50 nm, 600/50 nm and 700/72 nm.

Neuronal morphological analysis

All neurons used in this study were subjected to several measurements of their morphological characteristics. All images were captured as z-series with a Nikon T2i Inverted Confocal Microscope, as described above. Prior to analysis, NIH ImageJ was used to create a two-dimensional, background-subtracted maximum-projection image from the confocal z-series images for each neuron. Dendrite number was measured by quantifying the number of dendrite tips per neuron. Tips of any protrusion shorter than 5 μm were excluded. Dendritic length measurements were made by tracing from the cell body to the dendrite tip in ImageJ. Several morphological experiments were run in parallel and, where appropriate, controls were shared. For Sholl analysis, maximum-projection images were converted to binary and subjected to analysis in ImageJ. Concentric rings with a step size of 5 μm were used to quantify dendrite morphology as it relates to distance from the soma. Thresholds were assigned via the Auto Threshold tool in ImageJ. No significant differences between average thresholds of different conditions were observed. The range of condition threshold averages, on a scale of

0–4095, was 1179–1242. A one-way ANOVA followed by Tukey's test was used to determine significance. For all comparisons, $P \geq 0.6055$.

FRET image acquisition

Images were acquired using a Nikon A1 confocal microscope with a 63×1.4 NA oil immersion objective (Basic Research Science Building Microscopy Facility, Department of Genetics, UT MDACC). The images were collected using two lines of excitation (440 and 512 nm, solid-state lasers) and two different channels of emission. The intensity of fluorescence of CFP after CFP excitation at 440 nm (donor signal, I_{DD}) was obtained using a 485/35-nm bandpass emission filter. The intensity of fluorescence of YFP after excitation at 440 nm was measured using a 545/40-nm emission filter (raw FRET signal, I_{DA}). All images were collected using two-frame Kallman averaging, with a pixel size of $200\text{ nm} \times 200\text{ nm}$ (scan zoom of 1; frame size of 512×512 pixels; one frame per second). Detector gains, amplifier offsets, and laser power were adjusted to maximize the range of signal for each channel and were kept constant for all samples.

FRET image processing

Images were processed using NIS-Elements software. Initially, background was subtracted from all images based on the signal of noncellular regions. To obtain a ratio FRET image, we divided the signal of the FRET channel (I_{DA}) by that of the CFP channel (I_{DD}). All ratio ranges were kept constant among all the analyzed images. To obtain a dendrite:soma RhoA activity ratio profile for a neuron, the ratio FRET image intensity was measured from the center of each dendrite and divided by an equal number of intensities from the soma of the cell.

Statistical analysis

Data were analyzed using GraphPad Prism. Statistical significance for Sholl data were determined using a two-way ANOVA with Bonferroni post-hoc analysis. Significance for the comparisons in Fig. 4, E, F, H, and K and Fig. 6 D was determined using a two-tailed t test. For all other comparisons, a one-way ANOVA with Tukey's test was used. Data distribution was assumed to be normal, but this was not formally tested. Significance was assigned at $P < 0.05$.

Antibodies

All anti-HA, -Myc, and -FLAG (mouse monoclonal and rabbit polyclonal) were purchased from Sigma-Aldrich. The rabbit polyclonal delta-catenin antibody used for immunofluorescence was purchased from Sigma-Aldrich (catalog # HPA015077), while the mouse monoclonal delta-catenin antibody used for immunofluorescence and immunoblot analysis was purchased from BD Transduction Laboratories (catalog # 611537). The mouse monoclonal Magi1 antibody was purchased from Sigma-Aldrich (catalog # WH0009223M3). Pdlim5 antibodies were purchased from Thermo Fisher Scientific (polyclonal; catalog # 38–8800) and Sigma-Aldrich (monoclonal; catalog # WH0010611M1). The P-MAPK/CDK (PXS*P) antibody used in delta-catenin phosphorylation assays was purchased from Cell Signaling Technologies

(catalog # 23255). All secondary antibodies were purchased from Thermo Fisher Scientific.

Protein domain microarray

The protein domain microarray was conducted by the laboratory of Mark Bedford at the MD Anderson Protein Array and Analysis Core. A comprehensive library of human PDZ protein domains was cloned into a pGEX vector by Biomatik using gene synthesis to best optimize the open reading frames for bacterial expression. *Escherichia coli* was used to express the protein domains as GST fusions, which were purified using glutathione-Sepharose beads. The recombinant domains were arrayed onto nitrocellulose-coated glass slides (Oncyte vid slides, Grace Bio-Labs), using an Aushon 2470 pin microarrayer, as previously described (Espejo et al., 2002). The slides were probed with biotinylated delta-catenin PDZ-binding motif peptides (CPC Scientific). Following probing, fluorescent signal was detected with a GenePix 4200A Microarray Scanner (Molecular Devices). A total of four delta-catenin probes were used, with each of the phospho-probes generating similar results.

Sequences of delta-catenin probes

The sequences of delta-catenin probes are as follows: De-Phospho, Biotin-TSHYPASPDSWV; Phospho ($-3S \rightarrow E$), Biotin-TSHYPASPD-S(PO_3H_2)-WV; Phospho ($-6S \rightarrow E$), Biotin-TSHYPA-S(PO_3H_2)-PDSWV; and Phospho($-3S \rightarrow E$, $-6S \rightarrow E$), Biotin-TSHYPA-S(PO_3H_2)-PD-S(PO_3H_2)-WV.

Identification of critical residues in Magi1:delta-catenin and Pdlim5:delta-catenin complexes

Identification of the residues in the PDZ domains of Magi1 and Pdlim5 required to bind the PDZ-binding motif of delta-catenin was performed by our collaborator Xiaojiang Chen at the University of Southern California. To generate a rough model for prediction of peptide docking, a homology model for Magi1 PDZ5 was created using the SWISS-MODEL prediction server (Guex et al., 2009; Benkert et al., 2011; Biasini et al., 2014; Bienert et al., 2017) using chain B of the previously reported Magi1 PDZ1 structure (Zhang et al., 2007) that comparatively has a sequence identity of 33%. This solution was then used as input into the Rosetta FlexPepDock server (Raveh et al., 2010; London et al., 2011), using the placement of the bound E6 peptide as a relative starting point and using the default run options recommended by the server. Upon confirmation of model convergence, the resulting top solution was then energy minimized using the ROSETTARELAX application, with a thorough search completed using energy parameters guided by the Talaris2014 weighting. Relax parameters were chosen to optimize packing and bonding interactions, with mild constraints toward the input coordinates, and largely default options were used. The resulting minimized solution was then reported as the standard configuration within this manuscript.

Online supplemental material

Fig. S1 shows the similar localization patterns of exogenous phospho-mimic delta-catenin and phospho-null delta-catenin in dendrites of rat hippocampal neurons. Fig. S2 shows the

mapping of the delta-catenin-binding regions of Magil and Pdlim5 through the use of our GRA. Fig. S3 shows that the expression levels of Magil, Pdlim5, and delta-catenin increase throughout much of development in hippocampal neurons as well as the specificity and efficiency of shRNA-mediated KD of each of these three proteins. Fig. S4 shows that Magil and Pdlim5 expression each require the presence of delta-catenin to exert a significant impact on dendrite morphology in developing hippocampal neurons. Table S1 shows the full list of domains probed in the protein domain microarray, along with their respective signal intensities.

Acknowledgments

For helpful discussion and/or reagents, we thank Malgosia Kloc, Rachel Miller, Mark Corkins, Bridget DeLay, Vanja Stankic, Alexandra Blackburn, Kevin Stebbings, Steven Pelech, Swathi Arur, Bin Wang, Don Gibbons, Roxsan Manshour, Jeff Frost, Michael Zhu, George Eisenhoffer, Andrew Gladden, Jack Waymire, Darren Boehning, Eric Swindell, and Anna Marie Sokac. We also appreciate suggestions from members of the Texas Medical Center Cytoskeletal Super Group. The authors would like to acknowledge Dr. Andrey Tsvetkov, Ndidi Uzor, and Felix Moruno Manchon (UTHealth) for help with primary neuronal cultures.

Use of the A1-Nikon (confocal images) was made possible via the UT MDACC Department of Genetics NIH Instrumentation Grant 1S10OD024976-01 (A. Paulucci-Holtzhausen). Probing of arrayed PDZ domains was made possible via the UT MDACC Protein Array and Analysis Core CPRIT Grant RP180804 (M.T. Bedford). Assistance with DNA sequencing was provided from National Cancer Institute Core Grant CA-16672 to UT MDACC. This work was supported by NIH grants RO1GM107079 (P.D. McCrea), RO1GM129098 (L. Hodgson), and 1RO1MH115717 (P.D. McCrea and M.N. Waxham). P.D. McCrea also acknowledges an Ashbel Smith Professorship Award, and M.N. Waxham an endowment from the William Wheelless III Professorship.

The authors declare no competing financial interests.

Author contributions: P.D. McCrea planned the project and analyzed data with R. Baumert and M.N. Waxham. R. Baumert conducted experiments with delta-catenin, Magil, and Pdlim5 in HEK293 cells and primary neuron cultures. H. Ji generated delta-catenin, Magil, and Pdlim5 DNA constructs. L. Hodgson generated RhoA FRET biosensor. J. Arikath generated delta-catenin shRNA and shRNA-resistant constructs. M.T. Bedford and C. Sagum performed the protein domain microarrays. X. Chen and A. Wolfe modeled interactions of Magil and Pdlim5 with delta-catenin. A. Paulucci-Holtzhausen assisted with microscopy and performed STORM imaging. M.N. Waxham provided advice and prepared primary rat hippocampal neuron cultures. The manuscript was written by R. Baumert and P.D. McCrea, with commentary from all authors.

Submitted: 4 October 2019

Revised: 27 December 2019

Accepted: 21 August 2020

References

- Abu-Elneel, K., T. Ochiishi, M. Medina, M. Remedi, L. Gastaldi, A. Caceres, and K.S. Kosik. 2008. A delta-catenin signaling pathway leading to dendritic protrusions. *J. Biol. Chem.* 283:32781–32791. <https://doi.org/10.1074/jbc.M804688200>
- Andraea, L.C., and J. Burrone. 2015. Spontaneous Neurotransmitter Release Shapes Dendritic Arbors via Long-Range Activation of NMDA Receptors. *Cell Rep.* 10:873–882. <https://doi.org/10.1016/j.celrep.2015.01.032>
- Angulo, M.C., A.S. Kozlov, S. Charpak, and E. Audinat. 2004. Glutamate released from glial cells synchronizes neuronal activity in the hippocampus. *J. Neurosci.* 24:6920–6927. <https://doi.org/10.1523/JNEUROSCI.0473-04.2004>
- Arikath, J., I. Israely, Y. Tao, L. Mei, X. Liu, and L.F. Reichardt. 2008. Erbin controls dendritic morphogenesis by regulating localization of delta-catenin. *J. Neurosci.* 28:7047–7056. <https://doi.org/10.1523/JNEUROSCI.0451-08.2008>
- Arikath, J., I.F. Peng, Y.G. Ng, I. Israely, X. Liu, E.M. Ullian, and L.F. Reichardt. 2009. Delta-catenin regulates spine and synapse morphogenesis and function in hippocampal neurons during development. *J. Neurosci.* 29:5435–5442. <https://doi.org/10.1523/JNEUROSCI.0835-09.2009>
- Ballester-Rosado, C.J., M.J. Albright, C.S. Wu, C.C. Liao, J. Zhu, J. Xu, L.J. Lee, and H.C. Lu. 2010. mGluR5 in cortical excitatory neurons exerts both cell-autonomous and -nonautonomous influences on cortical somatosensory circuit formation. *J. Neurosci.* 30:16896–16909. <https://doi.org/10.1523/JNEUROSCI.2462-10.2010>
- Benkert, P., M. Biasini, and T. Schwede. 2011. Toward the estimation of the absolute quality of individual protein structure models. *Bioinformatics.* 27:343–350. <https://doi.org/10.1093/bioinformatics/btq662>
- Biasini, M., S. Bienert, A. Waterhouse, K. Arnold, G. Studer, T. Schmidt, F. Kiefer, T. Gallo Cassarino, M. Bertoni, L. Bordoli, et al. 2014. SWISS-MODEL: modelling protein tertiary and quaternary structure using evolutionary information. *Nucleic Acids Res.* 42(Web Server issue, W1). W252–8. <https://doi.org/10.1093/nar/gku340>
- Bienert, S., A. Waterhouse, T.A. de Beer, G. Tauriello, G. Studer, L. Bordoli, and T. Schwede. 2017. The SWISS-MODEL Repository—new features and functionality. *Nucleic Acids Res.* 45(D1):D313–D319. <https://doi.org/10.1093/nar/gkw1132>
- Buard, I., C.C. Steinmetz, T. Claudepierre, and F.W. Pfrieger. 2010. Glial cells promote dendrite formation and the reception of synaptic input in Purkinje cells from postnatal mice. *Glia.* 58:538–545. <https://doi.org/10.1002/glia.20943>
- Cerruti Mainardi, P. 2006. Cri du Chat syndrome. *Orphanet J. Rare Dis.* 1:33. <https://doi.org/10.1186/1750-1172-1-33>
- Charych, E.I., B.F. Akum, J.S. Goldberg, R.J. Jörnsten, C. Rongo, J.Q. Zheng, and B.L. Firestein. 2006. Activity-independent regulation of dendrite patterning by postsynaptic density protein PSD-95. *J. Neurosci.* 26:10164–10176. <https://doi.org/10.1523/JNEUROSCI.2379-06.2006>
- Chen, X., J.M. Levy, A. Hou, C. Winters, R. Azzam, A.A. Sousa, R.D. Leapman, R.A. Nicoll, and T.S. Reese. 2015. PSD-95 family MAGUKs are essential for anchoring AMPA and NMDA receptor complexes at the postsynaptic density. *Proc. Natl. Acad. Sci. USA.* 112:E6983–E6992. <https://doi.org/10.1073/pnas.1517045112>
- Cheung, Z.H., W.H. Chin, Y. Chen, Y.P. Ng, and N.Y. Ip. 2007. Cdk5 is involved in BDNF-stimulated dendritic growth in hippocampal neurons. *PLoS Biol.* 5. e63. <https://doi.org/10.1371/journal.pbio.0050063>
- Chung, H.J., J. Xia, R.H. Scannevin, X. Zhang, and R.L. Huganir. 2000. Phosphorylation of the AMPA receptor subunit GluR2 differentially regulates its interaction with PDZ domain-containing proteins. *J. Neurosci.* 20:7258–7267. <https://doi.org/10.1523/JNEUROSCI.20-19-07258.2000>
- Contreras-Vallejos, E., E. Utreras, D.A. Bórquez, M. Prochazkova, A. Terse, H. Jaffe, A. Toledo, C. Arruti, H.C. Pant, A.B. Kulkarni, et al. 2014. Searching for novel Cdk5 substrates in brain by comparative phosphoproteomics of wild type and Cdk5^{-/-} mice. *PLoS One.* 9. e90363. <https://doi.org/10.1371/journal.pone.0090363>
- Cruz-Martín, A., M. Crespo, and C. Portera-Cailliau. 2012. Glutamate induces the elongation of early dendritic protrusions via mGluRs in wild type mice, but not in fragile X mice. *PLoS One.* 7. e32446. <https://doi.org/10.1371/journal.pone.0032446>
- Danielson, E., N. Zhang, J. Metallo, K. Kaleka, S.M. Shin, N. Gerges, and S.H. Lee. 2012. S-SCAM/MAGI-2 is an essential synaptic scaffolding molecule for the GluA2-containing maintenance pool of AMPA receptors.

- J. Neurosci. 32:6967–6980. <https://doi.org/10.1523/JNEUROSCI.0025-12.2012>
- de Moor, M.H., S.M. van den Berg, K.J. Verweij, R.F. Krueger, M. Luciano, A. Arias Vasquez, L.K. Matteson, J. Derringer, T. Esko, N. Amin, et al; Genetics of Personality Consortium. 2015. Meta-analysis of Genome-wide Association Studies for Neuroticism, and the Polygenic Association With Major Depressive Disorder. *JAMA Psychiatry*. 72:642–650. <https://doi.org/10.1001/jamapsychiatry.2015.0554>
- Dong, X., K. Shen, and H.E. Bülow. 2015. Intrinsic and extrinsic mechanisms of dendritic morphogenesis. *Annu. Rev. Physiol.* 77:271–300. <https://doi.org/10.1146/annurev-physiol-021014-071746>
- Duman, J.G., S. Mulherkar, Y.K. Tu, K.C. Erikson, C.P. Tzeng, V.C. Mavratsas, T.S. Ho, and K.F. Tolias. 2019. The adhesion-GPCR BAI1 shapes dendritic arbors via Bcr-mediated RhoA activation causing late growth arrest. *eLife*. 8. e47566. <https://doi.org/10.7554/eLife.47566>
- Espejo, A., J. Côté, A. Bednarek, S. Richard, and M.T. Bedford. 2002. A protein-domain microarray identifies novel protein-protein interactions. *Biochem. J.* 367:697–702. <https://doi.org/10.1042/bj20020860>
- Espejo, A.B., G. Gao, K. Black, S. Gayatri, N. Veland, J. Kim, T. Chen, M. Sudol, C. Walker, and M.T. Bedford. 2017. PRMT5 C-terminal phosphorylation modulates a 14-3-3/PDZ interaction switch. *J. Biol. Chem.* 292:2255–2265. <https://doi.org/10.1074/jbc.M116.760330>
- Fischer, T.D., P.K. Dash, J. Liu, and M.N. Waxham. 2018. Morphology of mitochondria in spatially restricted axons revealed by cryo-electron tomography. *PLoS Biol.* 16. e2006169. <https://doi.org/10.1371/journal.pbio.2006169>
- Furrer, M.P., S. Kim, B. Wolf, and A. Chiba. 2003. Robo and Frazzled/DCC mediate dendritic guidance at the CNS midline. *Nat. Neurosci.* 6:223–230. <https://doi.org/10.1038/nn1017>
- Godenschwege, T.A., J.H. Simpson, X. Shan, G.J. Bashaw, C.S. Goodman, and R.K. Murphey. 2002. Ectopic expression in the giant fiber system of *Drosophila* reveals distinct roles for roundabout (Robo), Robo2, and Robo3 in dendritic guidance and synaptic connectivity. *J. Neurosci.* 22:3117–3129. <https://doi.org/10.1523/JNEUROSCI.22-08-03117.2002>
- Gottardi, C.J., and B.M. Gumbiner. 2004. Distinct molecular forms of β -catenin are targeted to adhesive or transcriptional complexes. *J. Cell Biol.* 167:339–349. <https://doi.org/10.1083/jcb.200402153>
- Govek, E.E., S.E. Newey, and L. Van Aelst. 2005. The role of the Rho GTPases in neuronal development. *Genes Dev.* 19:1–49. <https://doi.org/10.1101/gad.1256405>
- Gu, D., N.K. Tonthat, M. Lee, H. Ji, K.P. Bhat, F. Hollingsworth, K.D. Aldape, M.A. Schumacher, T.P. Zwaka, and P.D. McCrea. 2011. Caspase-3 cleavage links delta-catenin to the novel nuclear protein ZIFCAT. *J. Biol. Chem.* 286:23178–23188. <https://doi.org/10.1074/jbc.M110.167544>
- Guex, N., M.C. Peitsch, and T. Schwede. 2009. Automated comparative protein structure modeling with SWISS-MODEL and Swiss-PdbViewer: a historical perspective. *Electrophoresis*. 30(S1, Suppl 1):S162–S173. <https://doi.org/10.1002/elps.200900140>
- Hamad, M.I.K., Z.L. Ma-Högemeier, C. Riedel, C. Conrads, T. Veitinger, T. Habijan, J.N. Schulz, M. Krause, M.J. Wirth, M. Hollmann, et al. 2011. Cell class-specific regulation of neocortical dendrite and spine growth by AMPA receptor splice and editing variants. *Development*. 138:4301–4313. <https://doi.org/10.1242/dev.071076>
- Herrick, S., D.M. Evers, J.Y. Lee, N. Udagawa, and D.T. Pak. 2010. Postsynaptic PDLIM5/Enigma Homolog binds SPAR and causes dendritic spine shrinkage. *Mol. Cell. Neurosci.* 43:188–200. <https://doi.org/10.1016/j.mcn.2009.10.009>
- Hong, J.Y., I.H. Oh, and P.D. McCrea. 2016. Phosphorylation and isoform use in p120-catenin during development and tumorigenesis. *Biochim. Biophys. Acta*. 1863:102–114. <https://doi.org/10.1016/j.bbamcr.2015.10.008>
- Horiuchi, Y., M. Arai, K. Niizato, S. Iritani, E. Noguchi, T. Ohtsuki, M. Koga, T. Kato, M. Itokawa, and T. Arinami. 2006. A polymorphism in the PDLIM5 gene associated with gene expression and schizophrenia. *Biol. Psychiatry*. 59:434–439. <https://doi.org/10.1016/j.biopsych.2005.07.041>
- Horiuchi, Y., M. Ishikawa, N. Kaito, Y. Iijima, Y. Tanabe, H. Ishiguro, and T. Arinami. 2013. Experimental evidence for the involvement of PDLIM5 in mood disorders in hetero knockout mice. *PLoS One*. 8. e59320. <https://doi.org/10.1371/journal.pone.0059320>
- Ide, N., Y. Hata, M. Deguchi, K. Hirao, I. Yao, and Y. Takai. 1999. Interaction of S-SCAM with neural plakophilin-related Armadillo-repeat protein/delta-catenin. *Biochem. Biophys. Res. Commun.* 256:456–461. <https://doi.org/10.1006/bbrc.1999.0364>
- Ito, H., R. Morishita, K. Sudo, Y.V. Nishimura, Y. Inaguma, I. Iwamoto, and K. Nagata. 2012. Biochemical and morphological characterization of MAGI-1 in neuronal tissue. *J. Neurosci. Res.* 90:1776–1781. <https://doi.org/10.1002/jnr.23074>
- Ito, H., R. Morishita, I. Iwamoto, M. Mizuno, and K. Nagata. 2013. MAGI-1 acts as a scaffolding molecule for NGF receptor-mediated signaling pathway. *Biochim. Biophys. Acta*. 1833:2302–2310. <https://doi.org/10.1016/j.bbamcr.2013.06.005>
- Izawa, I., M. Nishizawa, Y. Tomono, K. Ohtakara, T. Takahashi, and M. Inagaki. 2002. ERBIN associates with p0071, an armadillo protein, at cell-cell junctions of epithelial cells. *Genes Cells*. 7:475–485. <https://doi.org/10.1046/j.1365-2443.2002.00533.x>
- Karlsson, R., L. Graae, M. Lekman, D. Wang, R. Favis, T. Axelsson, D. Galter, A.C. Belin, and S. Paddock. 2012. MAGI1 copy number variation in bipolar affective disorder and schizophrenia. *Biol. Psychiatry*. 71:922–930. <https://doi.org/10.1016/j.biopsych.2012.01.020>
- Kato, T., Y. Iwayama, C. Kakiuchi, K. Iwamoto, K. Yamada, Y. Minabe, K. Nakamura, N. Mori, K. Fujii, S. Nanko, et al. 2005. Gene expression and association analyses of LIM (PDLIM5) in bipolar disorder and schizophrenia. *Mol. Psychiatry*. 10:1045–1055. <https://doi.org/10.1038/sj.mp.4001719>
- Kaufmann, W.E., and H.W. Moser. 2000. Dendritic anomalies in disorders associated with mental retardation. *Cereb. Cortex*. 10:981–991. <https://doi.org/10.1093/cercor/10.10.981>
- Kim, S., and A. Chiba. 2004. Dendritic guidance. *Trends Neurosci.* 27:194–202. <https://doi.org/10.1016/j.tins.2004.02.011>
- Kim, K., A. Sirota, Y.H. Chen Yh, S.B. Jones, R. Dudek, G.W. Lanford, C. Thakore, and Q. Lu. 2002. Dendrite-like process formation and cytoskeletal remodeling regulated by delta-catenin expression. *Exp. Cell Res.* 275:171–184. <https://doi.org/10.1006/excr.2002.5503>
- Kim, H., J.R. Han, J. Park, M. Oh, S.E. James, S. Chang, Q. Lu, K.Y. Lee, H. Ki, W.J. Song, and K. Kim. 2008a. Delta-catenin-induced dendritic morphogenesis. An essential role of p190RhoGEF interaction through Akt1-mediated phosphorylation. *J. Biol. Chem.* 283:977–987. <https://doi.org/10.1074/jbc.M707158200>
- Kim, H., M. Oh, Q. Lu, and K. Kim. 2008b. E-Cadherin negatively modulates δ -catenin-induced morphological changes and RhoA activity reduction by competing with p190RhoGEF for δ -catenin. *Biochem. Biophys. Res. Commun.* 377:636–641. <https://doi.org/10.1016/j.bbrc.2008.10.030>
- Lasorella, A., and A. Iavarone. 2006. The protein ENH is a cytoplasmic sequestration factor for Id2 in normal and tumor cells from the nervous system. *Proc. Natl. Acad. Sci. USA*. 103:4976–4981. <https://doi.org/10.1073/pnas.0600168103>
- Lee, H.J., and J.J. Zheng. 2010. PDZ domains and their binding partners: structure, specificity, and modification. *Cell Commun. Signal.* 8:8. <https://doi.org/10.1186/1478-811X-8-8>
- Lee, M., H. Ji, Y. Furuta, J.I. Park, and P.D. McCrea. 2014. p120-catenin regulates REST and CoREST, and modulates mouse embryonic stem cell differentiation. *J. Cell Sci.* 127:4037–4051. <https://doi.org/10.1242/jcs.151944>
- Liang, Z., T. Ye, X. Zhou, K.O. Lai, A.K. Fu, and N.Y. Ip. 2015. Cdk5 Regulates Activity-Dependent Gene Expression and Dendrite Development. *J. Neurosci.* 35:15127–15134. <https://doi.org/10.1523/JNEUROSCI.1443-15.2015>
- Liu, F., X.H. Ma, J. Ule, J.A. Bibb, A. Nishi, A.J. DeMaggio, Z. Yan, A.C. Nairn, and P. Greengard. 2001. Regulation of cyclin-dependent kinase 5 and casein kinase 1 by metabotropic glutamate receptors. *Proc. Natl. Acad. Sci. USA*. 98:11062–11068. <https://doi.org/10.1073/pnas.191353898>
- Loerwald, K.W., A.B. Patel, K.M. Huber, and J.R. Gibson. 2015. Postsynaptic mGluR5 promotes evoked AMPAR-mediated synaptic transmission onto neocortical layer 2/3 pyramidal neurons during development. *J. Neurophysiol.* 113:786–795. <https://doi.org/10.1152/jn.00465.2014>
- London, N., B. Ravesh, E. Cohen, G. Fathi, and O. Schueler-Furman. 2011. Rosetta FlexPepDock web server—high resolution modeling of peptide-protein interactions. *Nucleic Acids Res.* 39(Web Server issue, SUPPL. 2):W249–53. <https://doi.org/10.1093/nar/gkr431>
- Lundby, A., A. Secher, K. Lage, N.B. Nordborg, A. Dmytryiev, C. Lundby, and J.V. Olsen. 2012. Quantitative maps of protein phosphorylation sites across 14 different rat organs and tissues. *Nat. Commun.* 3:876. <https://doi.org/10.1038/ncomms1871>
- Martinez, M.C., T. Ochiishi, M. Majewski, and K.S. Kosik. 2003. Dual regulation of neuronal morphogenesis by a δ -catenin-cortactin complex and Rho. *J. Cell Biol.* 162:99–111. <https://doi.org/10.1083/jcb.200211025>
- Martínez-Cerdeño, V. 2017. Dendrite and spine modifications in autism and related neurodevelopmental disorders in patients and animal models. *Dev. Neurobiol.* 77:393–404. <https://doi.org/10.1002/dneu.22417>

- Matter, C., M. Pribadi, X. Liu, and J.T. Trachtenberg. 2009. Delta-catenin is required for the maintenance of neural structure and function in mature cortex in vivo. *Neuron*. 64:320–327. <https://doi.org/10.1016/j.neuron.2009.09.026>
- Medina, M., R.C. Marinescu, J. Overhauser, and K.S. Kosik. 2000. Hemizygotosity of delta-catenin (CTNND2) is associated with severe mental retardation in cri-du-chat syndrome. *Genomics*. 63:157–164. <https://doi.org/10.1006/geno.1999.6090>
- Montgomery, J.M., P.L. Zamorano, and C.C. Garner. 2004. MAGUKs in synapse assembly and function: an emerging view. *Cell. Mol. Life Sci.* 61: 911–929. <https://doi.org/10.1007/s00018-003-3364-5>
- Morey, T.M., R. Roufayel, D.S. Johnston, A.S. Fletcher, and D.D. Mosser. 2015. Heat shock inhibition of CDK5 increases NOXA levels through miR-23a repression. *J. Biol. Chem.* 290:11443–11454. <https://doi.org/10.1074/jbc.M114.625988>
- Nakayama, A.Y., M.B. Harms, and L. Luo. 2000. Small GTPases Rac and Rho in the maintenance of dendritic spines and branches in hippocampal pyramidal neurons. *J. Neurosci.* 20:5329–5338. <https://doi.org/10.1523/JNEUROSCI.20-14-05329.2000>
- Neugebauer, K.M., K.J. Tomaselli, J. Lilien, and L.F. Reichardt. 1988. N-cadherin, NCAM, and integrins promote retinal neurogenesis on astrocytes in vitro. *J. Cell Biol.* 107:1177–1187. <https://doi.org/10.1083/jcb.107.3.1177>
- Nikolic, M., H. Dudek, Y.T. Kwon, Y.F. Ramos, and L.H. Tsai. 1996. The cdk5/p35 kinase is essential for neurite outgrowth during neuronal differentiation. *Genes Dev.* 10:816–825. <https://doi.org/10.1101/gad.10.7.816>
- Nusse, R., and H. Clevers. 2017. Wnt/ β -Catenin Signaling, Disease, and Emerging Therapeutic Modalities. *Cell*. 169:985–999. <https://doi.org/10.1016/j.cell.2017.05.016>
- Ohshima, T., M. Hirasawa, H. Tabata, T. Mutoh, T. Adachi, H. Suzuki, K. Saruta, T. Iwasato, S. Itohara, M. Hashimoto, et al. 2007. Cdk5 is required for multipolar-to-bipolar transition during radial neuronal migration and proper dendrite development of pyramidal neurons in the cerebral cortex. *Development*. 134:2273–2282. <https://doi.org/10.1242/dev.02854>
- Oliva, C., P. Escobedo, C. Astorga, C. Molina, and J. Sierralta. 2012. Role of the MAGUK protein family in synapse formation and function. *Dev. Neurobiol.* 72:57–72. <https://doi.org/10.1002/dneu.20949>
- Park, H., A. Váradi, H. Seok, J. Jo, H. Gilpin, C.G. Liew, S. Jung, P.W. Andrews, E. Molnár, and K. Cho. 2007. mGluR5 is involved in dendrite differentiation and excitatory synaptic transmission in NTERA2 human embryonic carcinoma cell-derived neurons. *Neuropharmacology*. 52: 1403–1414. <https://doi.org/10.1016/j.neuropharm.2007.01.021>
- Pertz, O., L. Hodgson, R.L. Klemke, and K.M. Hahn. 2006. Spatiotemporal dynamics of RhoA activity in migrating cells. *Nature*. 440:1069–1072. <https://doi.org/10.1038/nature04665>
- Polleux, F., T. Morrow, and A. Ghosh. 2000. Semaphorin 3A is a chemoattractant for cortical apical dendrites. *Nature*. 404:567–573. <https://doi.org/10.1038/35007001>
- Portera-Cailliau, C., D.T. Pan, and R. Yuste. 2003. Activity-regulated dynamic behavior of early dendritic protrusions: evidence for different types of dendritic filopodia. *J. Neurosci.* 23:7129–7142. Available at: <http://www.ncbi.nlm.nih.gov/pubmed/12904473>. <https://doi.org/10.1523/JNEUROSCI.23-18-07129.2003>
- Previtera, M.L., and B.L. Firestein. 2015. Glutamate affects dendritic morphology of neurons grown on compliant substrates. *Biotechnol. Prog.* 31: 1128–1132. <https://doi.org/10.1002/btpr.2085>
- Procko, C., and S. Shaham. 2010. Assisted morphogenesis: glial control of dendrite shapes. *Curr. Opin. Cell Biol.* 22:560–565. <https://doi.org/10.1016/j.ceb.2010.07.005>
- Raveh, B., N. London, and O. Schueler-Furman. 2010. Sub-angstrom modeling of complexes between flexible peptides and globular proteins. *Proteins*. 78:2029–2040. <https://doi.org/10.1002/prot.22716>
- Ren, B., X. Li, J. Zhang, J. Fan, J. Duan, and Y. Chen. 2015. PDLIM5 mediates PKC ϵ translocation in PMA-induced growth cone collapse. *Cell. Signal.* 27:424–435. <https://doi.org/10.1016/j.cellsig.2014.12.005>
- Schnell, E., M. Sizemore, S. Karimzadegan, L. Chen, D.S. Bredt, and R.A. Nicoll. 2002. Direct interactions between PSD-95 and stargazin control synaptic AMPA receptor number. *Proc. Natl. Acad. Sci. USA*. 99: 13902–13907. <https://doi.org/10.1073/pnas.172511999>
- Silverman, J.B., S. Restituito, W. Lu, L. Lee-Edwards, L. Khatri, and E.B. Ziff. 2007. Synaptic anchorage of AMPA receptors by cadherins through neural plakophilin-related arm protein AMPA receptor-binding protein complexes. *J. Neurosci.* 27:8505–8516. <https://doi.org/10.1523/JNEUROSCI.1395-07.2007>
- Söderberg, O., M. Gullberg, M. Jarvius, K. Ridderstråle, K.J. Leuchowius, J. Jarvius, K. Wester, P. Hydbring, F. Bahram, L.G. Larsson, et al. 2006. Direct observation of individual endogenous protein complexes in situ by proximity ligation. *Nat. Methods*. 3:995–1000. <https://doi.org/10.1038/nmeth947>
- Stiffler, M.A., V.P. Grantcharova, M. Sevecka, and G. MacBeath. 2006. Uncovering quantitative protein interaction networks for mouse PDZ domains using protein microarrays. *J. Am. Chem. Soc.* 128:5913–5922. <https://doi.org/10.1021/ja060943h>
- Sundell, G.N., R. Arnold, M. Ali, P. Naksukpaiboon, J. Orts, P. Güntert, C.N. Chi, and Y. Ivarsson. 2018. Proteome-wide analysis of phosphoregulated PDZ domain interactions. *Mol. Syst. Biol.* 14. e8129. <https://doi.org/10.15252/msb.20178129>
- Threadgill, R., K. Bobb, and A. Ghosh. 1997. Regulation of dendritic growth and remodeling by Rho, Rac, and Cdc42. *Neuron*. 19:625–634. [https://doi.org/10.1016/S0896-6273\(00\)80376-1](https://doi.org/10.1016/S0896-6273(00)80376-1)
- Turner, T.N., K. Sharma, E.C. Oh, Y.P. Liu, R.L. Collins, M.X. Sosa, D.R. Auer, H. Brand, S.J. Sanders, D. Moreno-De-Luca, et al. 2015. Loss of δ -catenin function in severe autism. *Nature*. 520:51–56. <https://doi.org/10.1038/nature14186>
- Urizar-Arenaza, I., N. Osinalde, V. Akimov, M. Puglia, L. Cadenas, F.M. Pinto, I. Muñoz-Hoyos, M. Gianzo, R. Matorras, J. Irazusta, et al. 2019. Phosphoproteomic and Functional Analyses Reveal Sperm-specific Protein Changes Downstream of Kappa Opioid Receptor in Human Spermatozoa. *Mol. Cell. Proteomics*. 18(Suppl 1):S118–S131. <https://doi.org/10.1074/mcp.RA118.001133>
- Vadodaria, K.C., C. Brakebusch, U. Suter, and S. Jessberger. 2013. Stage-specific functions of the small Rho GTPases Cdc42 and Rac1 for adult hippocampal neurogenesis. *J. Neurosci.* 33:1179–1189. <https://doi.org/10.1523/JNEUROSCI.2103-12.2013>
- Verbich, D., G.A. Prenosil, P.K. Chang, K.K. Murai, and R.A. McKinney. 2012. Glial glutamate transport modulates dendritic spine head protrusions in the hippocampus. *Glia*. 60:1067–1077. <https://doi.org/10.1002/glia.22335>
- Vrijenhoek, T., J.E. Buizer-Voskamp, I. van der Stelt, E. Strengman, C. Sabatti, A. Geurts van Kessel, H.G. Brunner, R.A. Ophoff, and J.A. Veltman. 2008. Genetic Risk and Outcome in Psychosis (GROUP) Consortium. 2008. Recurrent CNVs disrupt three candidate genes in schizophrenia patients. *Am. J. Hum. Genet.* 83:504–510. <https://doi.org/10.1016/j.ajhg.2008.09.011>
- Weed, S.A., A.V. Karginov, D.A. Schafer, A.M. Weaver, A.W. Kinley, J.A. Cooper, and J.T. Parsons. 2000. Cortactin localization to sites of actin assembly in lamellipodia requires interactions with F-actin and the Arp2/3 complex. *J. Cell Biol.* 151:29–40. <https://doi.org/10.1083/jcb.151.1.29>
- Yamasaki, T., H. Kawasaki, and H. Nishina. 2012. Diverse Roles of JNK and MKK Pathways in the Brain. *J. Signal Transduct.* 2012. 459265. <https://doi.org/10.1155/2012/459265>
- Yuan, L., E. Seong, J.L. Beuscher, and J. Arikath. 2015. δ -Catenin Regulates Spine Architecture via Cadherin and PDZ-dependent Interactions. *J. Biol. Chem.* 290:10947–10957. <https://doi.org/10.1074/jbc.M114.632679>
- Zhang, Y., J. Dasgupta, R.Z. Ma, L. Banks, M. Thomas, and X.S. Chen. 2007. Structures of a human papillomavirus (HPV) E6 polypeptide bound to MAGUK proteins: mechanisms of targeting tumor suppressors by a high-risk HPV oncoprotein. *J. Virol.* 81:3618–3626. <https://doi.org/10.1128/JVI.02044-06>
- Zhang, D., J.Y. Zhang, S.D. Dai, S.L. Liu, Y. Liu, N. Tang, and E.H. Wang. 2014. Co-expression of delta-catenin and RhoA is significantly associated with a malignant lung cancer phenotype. *Int. J. Clin. Exp. Pathol.* 7: 3724–3732.
- Zhou, J., U. Liyanage, M. Medina, C. Ho, A.D. Simmons, M. Lovett, and K.S. Kosik. 1997. Presenilin 1 interaction in the brain with a novel member of the Armadillo family. *Neuroreport*. 8:2085–2090. <https://doi.org/10.1097/00001756-199705260-00054>
- Zhu, Y.-B., W. Gao, Y. Zhang, F. Jia, H.L. Zhang, Y.Z. Liu, X.F. Sun, Y. Yin, and D.M. Yin. 2016. Astrocyte-derived phosphatidic acid promotes dendritic branching. *Sci. Rep.* 6:21096. <https://doi.org/10.1038/srep21096>

Supplemental material

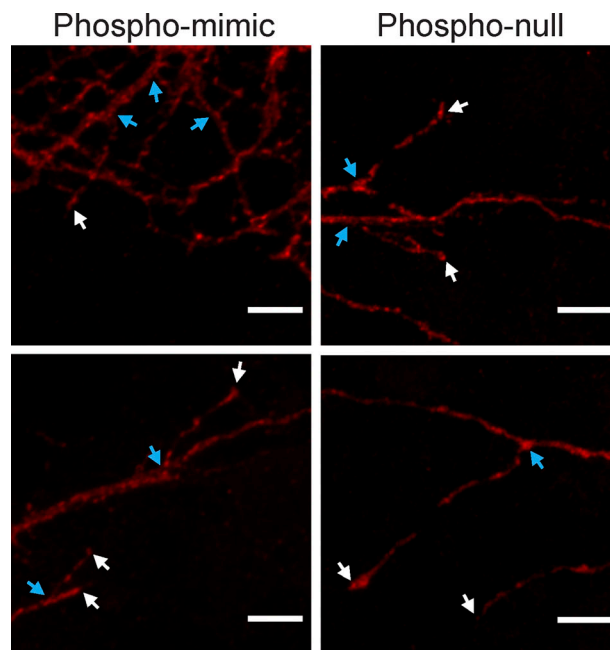


Figure S1. **Confocal images of dendrites of rat hippocampal neurons expressing HA-epitope-tagged phospho-mimic delta-catenin (delta-EE; duplicate left panels) versus HA-epitope-tagged phospho-null delta-catenin (delta-AA; duplicate right panels).** To facilitate determination of their sub-cellular localization, neurons were intentionally selected that exhibited low-level (faint) expression of either construct. At this resolution, fluorescent imaging of either mutant revealed no consistent/quantifiable difference in their localization to dendrite tips (white arrows) versus branch points (blue arrows). This is consistent with our hypothesis that pre-distributed delta-catenin along dendrites becomes transiently phosphorylated in response to local mGluR5 activation, promoting complex formation with Pdlim5 and branching (e.g., involving greater inhibition of RhoA), rather than delta-catenin becoming localized/translocated to the growing or future branch points only after the phosphorylation of its C-terminal PDZ-binding motif. Scale bars, 10 μ m.

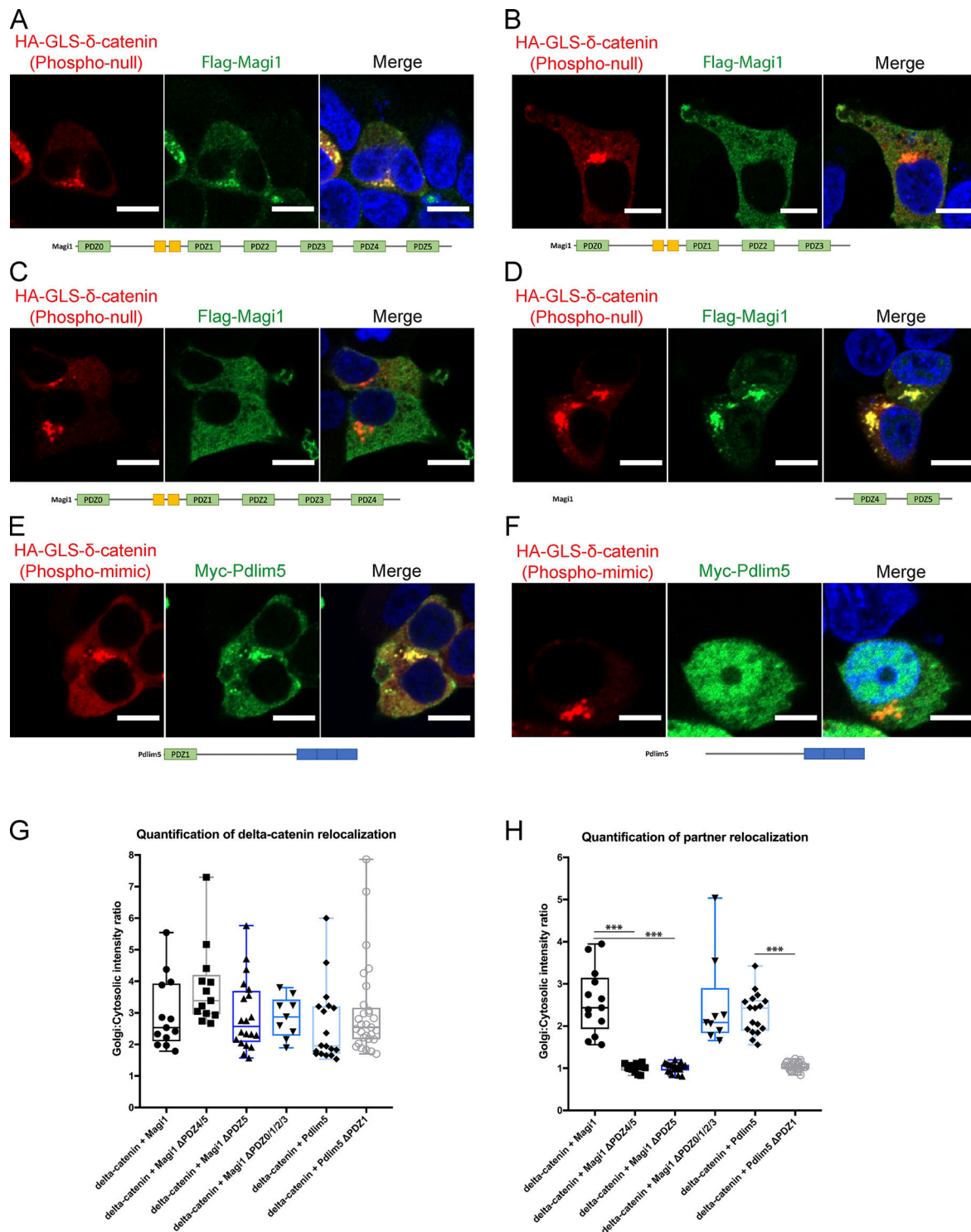


Figure S2. **Delta-catenin interacts with specific mapped domains of Magi1 and Pdlim5.** Through the application of our GRA in HEK293 cells, we validated our protein-domain microarray via domain mapping of Pdlim5 and Magi1. **(A–D)** Mapping of PDZ domain(s) of Magi1 required for interaction with delta-catenin. **(A)** Full-length Magi1 (green) co-relocalizes with delta-catenin (red) to Golgi body. **(B)** Deletion of PDZ4 and PDZ5 of Magi1 renders the protein unable to interact with delta-catenin, thereby preventing co-relocalization of Magi1 with delta-catenin (red) to the Golgi body. **(C)** Deletion of only PDZ5 of Magi1 also renders Magi1 (green) unable to co-relocalize to the Golgi, suggesting that PDZ5 is required for Magi1’s interaction with delta-catenin. **(D)** Expression of only PDZ4 and PDZ5 of Magi1 (green) successfully co-relocalizes to the Golgi with delta-catenin (red). **(E and F)** Validation and mapping of Pdlim5:delta-catenin interaction using a GRA in HEK293 cells. **(E)** Full-length Pdlim5 co-relocalizes with delta-catenin to Golgi body. **(F)** Deletion of the PDZ domain in Pdlim5 renders the protein unable to interact and co-relocalize with delta-catenin. **(G)** Quantification of delta-catenin localization in GRA. **(H)** Quantification of Magi1/Pdlim5 localization in GRA. Graphs represent cultures from at least two independent experiments. ***, $P \leq 0.0001$. Box plots indicate upper and lower quartiles (top/bottom of box), median value (center line of box), and the maximum/minimum values (whiskers). For G and H, significance was determined using a one-way ANOVA followed by Tukey’s test. Scale bars, 10 μ m.

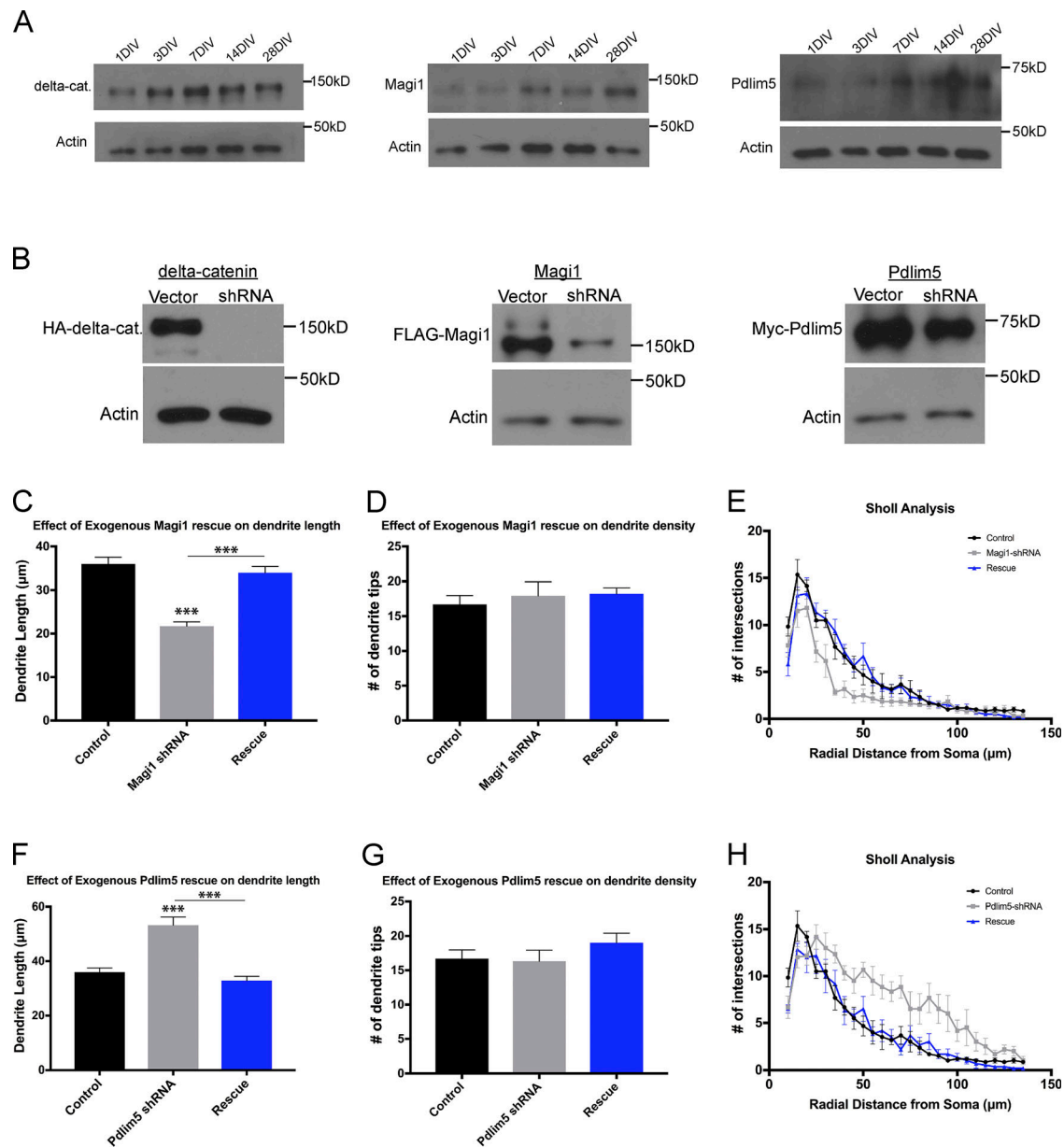


Figure S3. shRNA-mediated KD of delta-catenin, Magi1, and Pdlim5. (A) Immunoblots of delta-catenin, Magi1, and Pdlim5 from hippocampal neuron culture cell lysates from 1 DIV to 28 DIV. (B) Immunoblots of cell lysates from HEK293 cells coexpressing HA-delta-catenin, FLAG-Magi1, or Myc-Pdlim5 with either a control vector or the appropriate shRNA. We find that delta-catenin shRNA results in a near-complete loss of delta-catenin (~100% KD), while the Magi1 (~68% KD) and Pdlim5 (~60% KD) shRNAs produce slightly less complete KDs of their respective proteins. (C–E) Analysis of neurons expressing Magi1 shRNA compared with rescues (neurons expressing shRNA-KD and cDNA-overexpression constructs). (C) Expression of Flag-tagged Magi1 in Magi1 shRNA-expressing neurons resulted in a rescue of the shRNA dendrite length phenotype (control: $35.96 \pm 1.56 \mu\text{m}$; shRNA: $21.72 \pm 0.98 \mu\text{m}$; rescue: $33.94 \pm 1.44 \mu\text{m}$, $P < 0.0001$). (D) Expression of Magi1 cDNA in combination with Magi1 shRNA did not produce a significant impact on dendrite density (control: 16.69 ± 1.26 ; shRNA: 17.92 ± 2.01 ; rescue: $18.22 \pm 0.85 \mu\text{m}$, $P = 0.7911$). (E) Sholl analysis of Magi1 shRNA and rescue neurons reveals that rescue of the shRNA via expression of Magi1 results in a dendritic arborization pattern similar to that of controls. (F–H) Analysis of neurons expressing Pdlim5 shRNA compared with rescues (neurons expressing shRNA-KD and cDNA-overexpression constructs). (F) Expression of Myc-tagged Pdlim5 in Pdlim5 shRNA-expressing neurons resulted in a rescue of the shRNA dendrite length phenotype (control: $35.96 \pm 1.56 \mu\text{m}$; shRNA: $53.25 \pm 2.99 \mu\text{m}$; rescue: $32.83 \pm 1.57 \mu\text{m}$, $P < 0.0001$). (G) Expression of Pdlim5 cDNA in combination with Pdlim5 shRNA did not produce a significant impact on dendrite density (control: 16.69 ± 1.26 ; shRNA: 16.33 ± 1.61 ; rescue: 19.00 ± 1.41 , $P = 0.5931$). (H) Sholl analysis of Pdlim5 shRNA and rescue neurons reveals that rescue of the shRNA via expression of Pdlim5 results in a dendritic arborization pattern similar to that of controls. For C, D, F, and G, $n \geq 9$ neurons. For E and H, $n = 6$. ***, $P \leq 0.0001$. Error bars indicate SEM. For C, D, F, and G, significance was determined using a one-way ANOVA followed by Tukey's test. For E and H, a two-way ANOVA with Bonferroni post-hoc analysis was used.

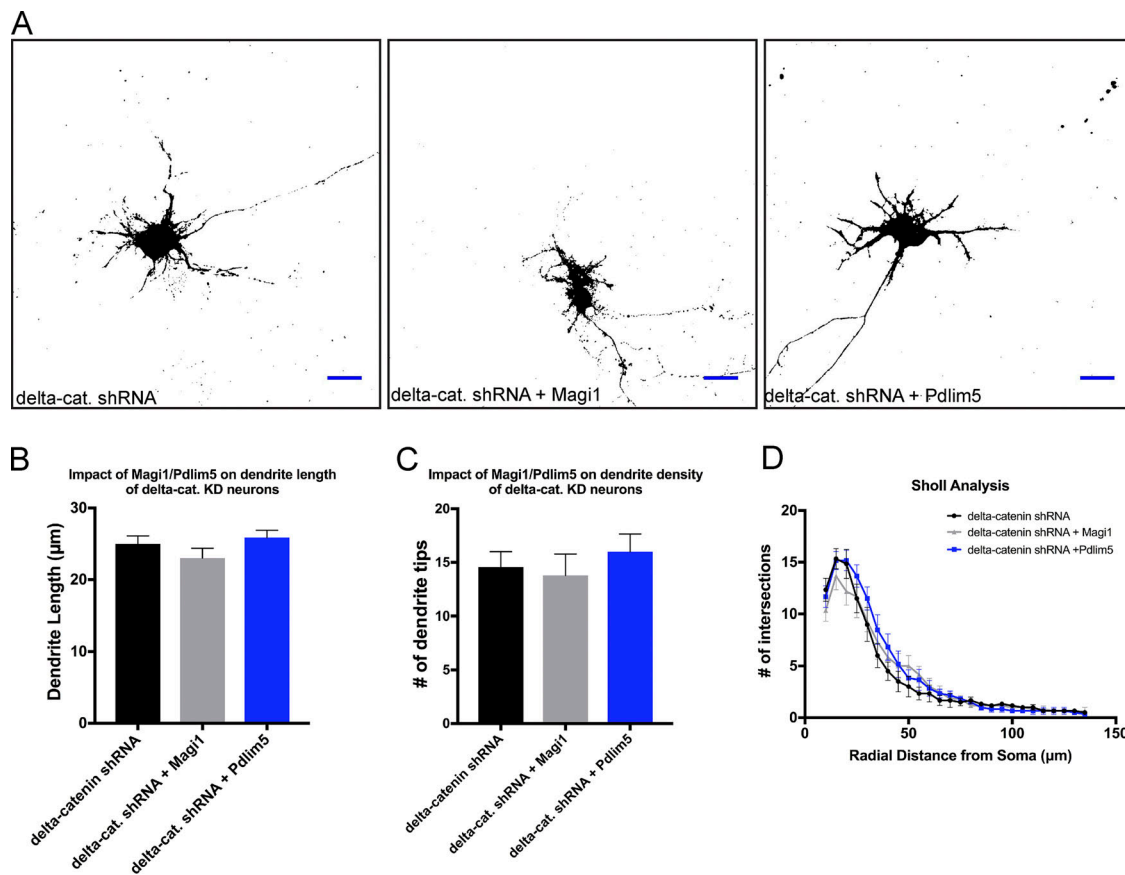


Figure S4. **Magi1 and Pdlim5 require delta-catenin to significantly affect dendrite morphology.** (A) Representative images of 7-DIV primary rat hippocampal neurons expressing delta-catenin shRNA alone and in combination with Magi1 or Pdlim5. (B–D) Analysis of neurons expressing delta-catenin shRNA alone compared with neurons expressing a combination of delta-catenin shRNA and either Magi1 or Pdlim5. (B) Expression of exogenous Magi1 or Pdlim5 in delta-catenin shRNA-expressing neurons fails to generate any impact on dendrite length (delta-cat. shRNA: 24.98 ± 1.13 μm; delta-cat. shRNA + Magi1: 23.01 ± 1.38 μm, $P = 0.4753$; delta-cat. shRNA + Pdlim5: 25.87 ± 1.03 μm, $P = 0.8435$). (C) Expression of exogenous Magi1 or Pdlim5 in delta-catenin shRNA-expressing neurons fails to generate any impact on dendrite density (delta-cat. shRNA: 14.56 ± 1.43; delta-cat. shRNA + Magi1: 13.78 ± 1.99, $P = 0.9398$; delta-cat. shRNA + Pdlim5: 16.00 ± 1.64, $P = 0.8127$); $n \geq 9$ neurons. (D) Sholl analysis of neurons expressing delta-catenin shRNA, delta-cat. shRNA + Magi1, and delta-cat. shRNA + Pdlim5 reveals that expression of either Magi1 or Pdlim5 in delta-catenin KD neurons generates very little impact on the morphology of the dendritic tree; $n = 6$. Error bars indicate SEM. For B and C, significance was determined using a one-way ANOVA followed by Tukey’s test. For D, a two-way ANOVA with Bonferroni post-hoc analysis was used. Scale bars, 20 μm.

Provided online is a table in an Excel file. Table S1 shows the full list of domains probed in the protein domain microarray, along with their respective signal intensities.